Revision 3

Word Count: 8058 (not including references) + 519 (figure captions) = 8577

Fluids in the Shallow Mantle of Southeastern Australia: Insights from Phase Equilibria

William M. Lamb, Department of Geology and Geophysics, Texas A&M University, College Station, TX 77843

Lindsey E. Hunt, Oklahoma Geological Survey, University of Oklahoma, Norman, OK 73019

Robert K. Popp[1], Department of Geology and Geophysics, Texas A&M University, College Station, TX. 77843

1. Present address: 1130 Spangler Mill Rd., Floyd, VA, 24091

This is the peer-reviewed, final accepted version for American Mineralogist, published by the Mineralogical Society of America.
The published version is subject to change. Cite as Authors (Year) Title. American Mineralogist, in press.
DOI: https://doi.org/10.2138/am-2022-8735. http://www.minsocam.org/

Abstract

Small amounts of water (10s to 100s of ppm) can have a profound effect on the properties of mantle peridotites, including viscosities, conductivities, and melting temperatures. Measuring the water content of nominally anhydrous minerals (NAMs) has provided insight into the amounts of water contained within mantle rocks. However, converting from NAM water contents to the activity of H_2O is non-trivial. Equilibria involving amphibole can be used to determine values of the activity of H_2O (aH_2O) at the time of mineral equilibration. This approach yields low values of the activity of H_2O (< 0.3) for four peridotite xenoliths from Southeastern Australia. These four xenoliths also record values of oxygen fugacity (fO_2) that range from -0.2 to -1.2 (Log units relative to FMQ). All these values of fO_2 are inconsistent with the presence of a CH_4-rich fluid (too oxidizing), and the lowest value of oxygen fugacity, as recorded by one sample, is inconsistent with the presence of a CO_2-rich fluid.

Keywords: mantle fluids, amphibole, peridotite, nominally anhydrous minerals, H_2O, CO_2

Introduction

The earth's mantle is a significant reservoir of carbon and hydrogen and, therefore, it likely plays an important role in whole-earth cycling of fluid species such as CO_2 (Black and Gibson, 2019; Dasgupta and Hirschmann, 2010; Hazen and Schiffries, 2013; Howell et al., 2020; Kelemen and Manning, 2015) and H_2O (Karlsen et al., 2019; Korenaga et al., 2017; Peslier et al., 2017). A fluid, as defined herein, is a volatile-rich phase likely dominated by C-, O-, and/or H-bearing components. At the pressures (P), temperatures (T) and oxygen fugacities typical of the earth's uppermost mantle the dominant hydrogen-bearing component of a lithostatically pressured C-O-H fluid phase, if a separate fluid phase is present, would be H_2O or, for relatively reducing conditions, CH_4 (Kang et al., 2017; Wood et al., 1990). However, H_2O reduces the melting temperature of peridotite and, therefore, rather than an H_2O-dominated fluid, mantle rocks with significant hydrogen may melt, depending, of course, on the P-T conditions (Asimow and Langmuir, 2003; Gaetani and Grove, 1998; Green, 2015; Green et al., 2014; Hirschmann, 2006). A melt phase may, therefore, be a H_2O-bearing phase in equilibrium with mantle peridotites. Hydrogen, residing in the earth's mantle may be bound in the structure of hydrous phases such as amphibole (Kovacs et al., 2021; Niida and Green, 1999; Popp and Bryndzia, 1992; Selway et al., 2015), and in nominally anhydrous minerals (NAMs), including olivine, pyroxene, and garnet. NAMs may constitute the largest reservoir of H in the earth's mantle (Chin and Palin, 2022; Demouchy and Bolfan-Casanova, 2016; Gibson et al., 2020; Ingrin and Skogby, 2000; Peslier et al., 2017; Peslier et al., 2010). The H in mineral phases, both hydrous and nominally anhydrous, or in mantle magmas, may be bound to oxygen and is typically quantified in terms of the amount of H_2O. The presence of H, or H_2O, in these phases does not require the presence of a lithostatically-pressured fluid phase. However, some authors have adopted the generic term

This is the peer-reviewed, final accepted version for American Mineralogist, published by the Mineralogical Society of America.
The published version is subject to change. Cite as Authors (Year) Title. American Mineralogist, in press.
DOI: https://doi.org/10.2138/am-2022-8735. http://www.minsocam.org/

"water" to describe the H, OH, or H_2O contents of mantle rocks, even if these hydrogen-bearing species are entirely contained within hydrous or nominally anhydrous mineral phases. We adopt that terminology here, although we may use other terms (e.g., the OH content of amphibole, or H_2O content of nominally anhydrous phases) if a more accurate term is deemed useful.

Water, even in trace amounts, has a significant effect on the physical properties of mantle rocks including electrical conductivity (Karato, 2019; Selway, 2019; Tarits et al., 2004; Wang et al., 2008), rheology (Masuti et al., 2019; Mei and Kohlstedt, 2000a; Mei and Kohlstedt, 2000b) and the pressure-temperature conditions of mantle melting and the compositions of the melts generated (Gaetani and Grove, 1998; Green, 2015; Green et al., 2014). This is often the case even if H_2O is not present as a component in a lithostatically pressured fluid phase. Experiments on olivine, for example, have shown that only small amounts of water are needed to produce "water weakening" (Demouchy et al., 2012; Faul et al., 2016; Girard et al., 2013; Jung et al., 2006; Karato and Jung, 1998; Mei and Kohlstedt, 2000a; Mei and Kohlstedt, 2000b; Tielke et al., 2017; Wallis et al., 2019). Consequently, a complete understanding of mantle rheology depends on our ability to estimate values of $a H_2O$ for different regions of the mantle.

Direct measurement of the H_2O contents of the nominally anhydrous minerals (NAMs) contained in mantle samples indicate that mantle pyroxenes contain approximately 30 to 1100 ppm H_2O by weight, mantle olivines contain approximately 4 to 400 wt.-ppm H_2O, and mantle garnets contain approximately 0 to 600 wt.-ppm H_2O (Bell and Rossman, 1992; Beran and Libowitzky, 2006; Demouchy and Bolfan-Casanova, 2016; Peslier, 2010; Peslier et al., 2017; Skogby, 2006). Relating these water contents to mantle properties such as viscosity and melting temperatures requires conversion of H_2O contents to values the fugacities (f) or activities of H_2O ($a H_2O$). Unfortunately, the link between H content of any particular NAM and the value of $a H_2O$ is not

104 perfectly understood. The H contents of pyroxenes, for example, do vary with aH_2O (Mierdel and
105 Keppler, 2004; Stalder et al., 2008), but the H contents also vary significantly with the amounts of
106 certain cations, such as Al in orthopyroxene (Mierdel et al., 2007; Stalder et al., 2005). Additional
107 experimental studies are necessary before pyroxene H contents can be used to determine values of
108 aH_2O. In contrast to mantle pyroxenes, the relation between the H contents of mantle olivine and
109 aH_2O is relatively well understood and is not only a function of the aH_2O, but also oxygen fugacity
110 (fO_2), pressure (P), temperature (T) and crystal chemistry (for example Al, Ti, and Fe contents,
111 although some of these chemical terms are negligible; Gaetani et al., 2014; Mosenfelder et al.,
112 2006; Tollan et al., 2017; Zhao et al., 2004). Thus, a value of aH_2O can be estimated from the H
113 content of a mantle olivine if P, T, fO_2 and the olivine chemical composition have been
114 determined.

115 Throughout this publication we typically report values of the activity for H_2O and fugacity
116 for O_2. This usage is consistent with previous literature as values related to chemical potential of
117 oxygen are often reported in terms of fugacity (e.g., Miller et al., 2016; Wood et al., 1990;
118 Woodland et al., 1992), and H_2O is often reported in terms of activity (e.g., Bonadiman et al.,
119 2014; Gentili et al., 2015; Lamb and Popp, 2009; Lamb and Valley, 1988; Phillips, 1980).
120 However, given that the activity of any given species (a_i) is proportional to the fugacity of that
121 species, such that $a_i = f_i/f_i^\circ$ (where f_i° is the fugacity of the pure fluid species i at the P and T of
122 interest), these terms are directly related.

123 Fluid-buffering equilibria have been applied to estimate the activities (fugacities) of various
124 fluid species. For example, oxygen fugacities have been estimated for mantle xenoliths and
125 orogenic peridotite massifs (alpine peridotites) interpreted to be of mantle origin (Miller et al.,
126 2016; Stagno et al., 2013; Wood et al., 1990; Woodland and Koch, 2003; Woodland et al., 1992).

In the upper mantle, these values typically range from 2 to 3 log units above (more oxidizing) to approximately 2 log units below (more reducing) than the fayalite-magnetite-quartz (FMQ) oxygen buffer (Bryndzia and Wood, 1990; Frost and McCammon, 2008; Ionov and Wood, 1992; Miller et al., 2016; Wood et al., 1990; Woodland et al., 1992). In the presence of graphite (or diamond) it is possible to calculate the activities (fugacities) of fluid species in the C-O-H system (CO_2, H_2O, CH_4, etc.) for a value of the oxygen fugacity if a lithostatically pressured fluid (volatile) phase is present. These calculations have been performed for both crustal (Chu and Ague, 2013; Connolly and Cesare, 1993; Lamb and Valley, 1984; Lamb and Valley, 1985) and mantle (Blundy et al., 1991; Bryndzia and Wood, 1990; Goncharov et al., 2012; Hunt and Lamb, 2019; Kang et al., 2017; Wood et al., 1990) rocks. Importantly, as first demonstrated by Lamb and Valley (1984; 1985), these calculations of fluids speciation in the C-O-H system can be performed on samples without a pure carbon species (e.g., graphite or diamond), in which case values of fO_2 put limits on the activities of various species. For example, minimum values of aH_2O and maximum values of aCO_2 have been estimated in this manner in both mantle and crustal rocks (Hunt and Lamb, 2019; Kang et al., 2017; Lamb and Valley, 1984; Lamb and Valley, 1985).

The activity of H_2O in the mantle has been estimated for amphibole-bearing peridotites (Gentili et al., 2015; Ghent et al., 2019; Hunt and Lamb, 2019; Kang et al., 2017; Lamb and Popp, 2009; Popp et al., 2006). These studies typically yield values of aH_2O that are less than approximately 0.3, although one sample from Antarctica yields a value of approximately 0.8 (Gentili et al., 2015). This paper applies mineral equilibria to amphibole bearing mantle xenoliths from Eastern Australia to further explore the use of phase equilibria to constrain values of aH_2O and fO_2. Determining values of aH_2O will, for example, provide some constraints on certain mantle properties, such as rheology and conductivity, as these depend, in part, on fH_2O. Existing

experimentally derived relations permit estimates of olivine H_2O-contents from values of fH_2O (Gaetani et al., 2014; Mosenfelder et al., 2006; Padron-Navarta and Hermann, 2017; Zhao et al., 2004) and, therefore, provide a manner to compare the water content from Eastern Australia with measured water contents from mantle samples collected from a variety of other locations (Beran and Libowitzky, 2006; Bolfan-Casanova, 2005; Chin and Palin, 2022; Peslier, 2010; Peslier et al., 2017). This paper also applies mineral equilibria to estimate values of fO_2 which can permit further insight into mantle conditions and fluid regimes at the time of mineral equilibration in these samples (Frost and McCammon, 2008; Hunt and Lamb, 2019; Kang et al., 2017; Lamb and Popp, 2009; Wood et al., 1990).

Sample Description and Mineralogy

Four xenoliths from Eastern Australia have been analyzed as part of this study (samples provided by Dr. Suzanne O'Reilly). These four samples (GN9912, GN9913, BM9912, BM9915) are from the Bullenmerri and Gnotuk Maars (Figure 1), which is an area that has been described in detail by Griffin et al. (1984) and O'Reilly and Griffin (1987; 1985; 1988). These samples are olivine-rich (> 60%) and contain varying amounts of pyroxene, amphibole, and spinel. The amphibole grains in these samples typically occur in multi-grain aggregates that often surround grains of spinel or clinopyroxene (Figure 2).

Samples from this same location, with similar textures and amphibole compositions, have been described by O'Reilly and Griffin (1988) who argue that amphiboles formation is likely related to metasomatism. In this case, fluids related to the intrusion of mafic magmas interacted with mantle minerals, particularly spinel, and the resulting reactions produced amphibole and, in some cases, other minerals (Griffin et al., 1988; O'Reilly and Griffin, 1988). This interpretation

is consistent with the observation that amphiboles often rim spinel grains with embayed margins, as shown in Figure 2 (see also, Griffin et al., 1988; O'Reilly and Griffin, 1988).

Although previous studies indicate that the amphiboles in question likely formed via metasomatism (O'Reilly and Griffin, 1988), it is not the goal of this paper to infer the composition of these fluid. The timing of the metasomatic event relative to xenolith emplacement is, for the samples examined in this study, unclear. Consequently, these rocks may have resided in the mantle for sufficient time to re-equilibrate under P-T conditions that were significantly different from the conditions of metasomatism. Our results provide insight into the fugacities of fluid components at the time the minerals last equilibrated, perhaps just prior to their emplacement at the earth's surface.

Analytical Methods

The chemical compositions of co-existing olivine, orthopyroxene, clinopyroxene, spinel, and amphibole were characterized using a Cameca SX-50 electron microprobe (EMP) located at Texas A&M University. Operating conditions for the EMP typically included an accelerating voltage of 15 kV, and, in the case of anhydrous phases (e.g., olivine, spinel and pyroxenes), a 20 nA beam current and a 1μm beam diameter. Amphibole grains were analyzed using a lower beam current of 10 nA and a larger beam diameter of 10 μm to minimize electron-beam induced diffusion of light elements, particularly H and F. The counting times for all phases ranged from 30-60 s for major elements and up to 120 s for minor elements. Core-to-rim traverses were performed to quantify any potential chemical variability within mineral grains. In addition to the traverses, several individual grains of each mineral were also analyzed in each sample to confirm homogeneity among mineral grains. Natural and synthetic mineral standards were used for

196 calibration. Mineral analyses, as well as normalized mineral formulae, for all samples can be
197 found in the Electronic Supplement.

198 Minerals were normalized as follows, with the appropriate number of cations denoted in
199 parentheses: olivine (3), pyroxenes (4), and spinel (3). The determination of values of $Fe^{3+}/\Sigma Fe$
200 (where $\Sigma Fe = Fe^{3+} + Fe^{2+}$) for these minerals was accomplished using a variety of methods given
201 that conventional EMP analyses cannot differentiate between the two valence states of Fe. The
202 amount of Fe^{3+} in olivine is often considered to be negligible (Canil and ONeill, 1996; Woodland
203 et al., 2006), and one study that did detect Fe^{3+} in olivine from a spinel lherzolite xenolith reports
204 a $Fe^{3+}/\Sigma Fe$ value of only 0.03 (Ejima et al., 2018). Thus, all Fe in the olivines analyzed for this
205 study is assumed to be Fe^{2+}. Accurate values of $Fe^{3+}/\Sigma Fe$ can be determined for spinels from
206 charge balance by using secondary standards with known values of $Fe^{3+}/\Sigma Fe$ (Wood and Virgo,
207 1989). For our samples, the value of $Fe^{3+}/\Sigma Fe$ in spinel, as estimated from charge balance, was
208 corrected based on analyses of secondary spinel standards, obtained from B. Wood (Ionov and
209 Wood, 1992; Wood and Virgo, 1989), which have values of $Fe^{3+}/\Sigma Fe$ that have been previously
210 determined using Mossbauer spectroscopy (Wood and Virgo, 1989) .

211 Determining values of $Fe^{3+}/\Sigma Fe$ for pyroxenes via charge balance is challenging given
212 statistical uncertainty (Canil and ONeill, 1996; Dyar et al., 1989), although careful analyses
213 indicate this approach may provide useful values for orthopyroxene (Hunt and Lamb, 2019). Thus,
214 we have estimated the value of $Fe^{3+}/\Sigma Fe$ for pyroxenes using two methods: (1) charge balance,
215 where $Fe^{3+} = Al^{IV} - Al^{VI} - 2Ti - Cr + Na$ and, (2) assuming that all Fe is Fe^{2+}. This approach permits
216 an examination of the sensitivity of various estimates, for example temperature estimates
217 (described below), to changes in the value of $Fe^{3+}/\Sigma Fe$ in pyroxenes.

Complete characterization of amphibole chemistry requires determination of: (1) the H_2O content, (2) the value of $Fe^{3+}/\Sigma Fe$, and (3) the fraction of the A-site that is vacant. Conventional microprobe analyses do not provide this information, however, it has been demonstrated that the value of $Fe^{3+}/\Sigma Fe$, the concentrations of other cations (e.g., Ti), and the oxy-content of mantle amphiboles are correlated (King et al., 1999; Lamb and Popp, 2009; Popp et al., 1995a). Given this relation, and a value for $Fe^{3+}/\Sigma Fe$, it is possible to determine the amphibole oxy-content and the A-site occupancy by requiring the resulting formula to charge balance (Lamb and Popp, 2009). This method begins with normalizing the EMP analysis of an amphibole to 16 cations (i.e., no vacancies). Given a value of $Fe^{3+}/\Sigma Fe$ it is possible to calculate the total positive charge for this amphibole normalization (this is the maximum possible positive charge for a given value of $Fe^{3+}/\Sigma Fe$ as this amphibole formula is vacancy free). We then apply the relation that that describes the correlation between the amount of oxygen in the O3 (hydroxyl) site and the amounts of other cations. For this study, we chose the relation $Fe^{3+} + Ti = O$ (Popp et al., 1995a), in which Fe^{3+}, Ti, and O are concentrations of these elements reported as atoms per formula unit, and the O represents the amount of oxygen in the hydroxyl site that is not bound to hydrogen (the oxy-component). Given the amounts of O, OH, F, and Cl in the hydroxyl site, as well as an additional 22 oxygens, it is possible to calculate the total negative charge of the resulting mineral formula. The result of this normalization typically does not charge balance, with the total positive charge greater than the total negative charge. In this case, the number of cations is reduced by a very small amount, which results in a small A-site vacancy, and the entire calculation is repeated. This iterative approach continues until charge balance is achieved.

Given the relatively small Fe-content contained in the amphiboles analyzed for this study, it was not possible to determine accurate values of $Fe^{3+}/\Sigma Fe$ using the EMP-based method

This is the peer-reviewed, final accepted version for American Mineralogist, published by the Mineralogical Society of America.
The published version is subject to change. Cite as Authors (Year) Title. American Mineralogist, in press.
DOI: https://doi.org/10.2138/am-2022-8735. http://www.minsocam.org/

described by Lamb et al. (2012). Thus, we chose to normalize the amphiboles using the method described in the previous paragraph, assuming both the maximum ($Fe^{3+}/\Sigma Fe = 1$) and minimum ($Fe^{3+}/\Sigma Fe = 0$) values possible. A value of zero (0) for $Fe^{3+}/\Sigma Fe$ will yield a maximum value for the amphibole OH content which, in turn, will yield a maximum value of aH_2O when estimated using amphibole dehydration equilibria. Similarly, a value of one (1) for $Fe^{3+}/\Sigma Fe$ will yield minimum value for the amphibole OH content (maximum oxy-content) which, in turn, will yield a minimum value of aH_2O. The maximum OH contents, reported as XOH (the fraction of the hydroxyl site occupied by OH) range from 0.92 to 0.97, while the minimum values ranged from 0.71 to 0.77. The amphibole compositions listed in the Electronic Supplement include: (1) a preliminary estimate of the H_2O content based on a simplified normalization for each analysis, and (2) an estimate of XOH for average amphibole compositions that is based on the normalization scheme described here and by Lamb and Popp (2009). It is this second value, based on mineral averages, that was used to estimate values of aH_2O.

Electron microprobe analyses reveal that the chemical compositions of olivine and amphibole from all four Australian samples are relatively homogeneous. Clinopyroxene and orthopyroxene are also largely homogeneous, but sometimes exhibit minor core to rim chemical variation, with a broad homogenous core and an Al-depleted, Si-rich rim (Figure 3). The average Cr # for the spinel grains is 0.31 (Cr# = Cr/(Cr+Al)) and spinels typically exhibit chemical zonation with rims relatively enriched in Cr and depleted in Al (Figure 3). The olivine Mg# for the four samples from Eastern Australia range from 0.88 to 0.91 (where Mg# = Mg/(Mg+ Fe)).

Estimation of Pressure and Temperature

Estimating values of aH_2O and fO_2 using mineral equilibria requires an estimate of the pressure (P) and temperature (T) of mineral equilibration to be determined for each sample. Two-

pyroxene geothermometry has been widely applied in mantle rocks (e.g., Nimis and Grutter, 2010), and was applied here to estimate temperature for all samples. Numerous versions of the two-pyroxene geothermometer have been calibrated for a variety of pyroxene compositions (Brey and Köhler, 1990; Taylor, 1998; Wells, 1977), however, geothermometers are often limited to a range of T, P and/or pyroxene compositions (e.g., Nimis and Grutter, 2010). Thus, the accuracy of temperature estimates depends, in part, on choosing the most appropriate geothermometer.

For this study, the two-pyroxene geothermometer of Taylor (1998) (T98) was used to estimate T. The choice of this thermometer was guided by Nimis & Grütter (2010), who favor the T98 formulation because it more accurately reproduces temperatures of experiments designed to yield equilibrium compositions of co-existing pyroxenes. Furthermore, Nimis & Grütter (2010) suggest that T estimates using T98 should be consistent with two other formulations of the pyroxene geothermometer, including the enstatite-in-Cpx thermometer of Nimis & Taylor (2000) (NT) and Ca-in-opx thermometer of Brey and Kohler (1990) (BK) as modified by Nimis & Grütter (2010) (BKNG). Thus, we have compared the results of four geothermometers (T(98), BK, NT, BKNG; Table 1) as a further test of mineral equilibration and to determine if the temperatures are accurate to ± 50 ˚C, as indicated by Taylor (1998).

In some cases, accurate temperature estimates from conventional thermobarometry may require determining values of $Fe^{3+}/\Sigma Fe$ in Fe-bearing minerals, including pyroxenes. The sensitivity of our temperature estimates to differences in $Fe^{3+}/\Sigma Fe$ was evaluated by determining two-pyroxene temperatures using two methods, described previously (charge balance and total Fe is Fe^{2+}), to determine values of $Fe^{3+}/\Sigma Fe$ in pyroxenes. Ultimately, the choice of whether to use charge balance or to consider all Fe as Fe^{2+} has no impact on our T estimates using either the T98, or the BKNG formulations. However, the maximum difference in temperature calculated using

these two methods with the NT formulation is 20 ˚C. This small T difference indicates that the two-pyroxene thermometer, as applied to mantle rocks, is relatively insensitive to uncertainties in $Fe^{3+}/\Sigma Fe$, a conclusion supported by previous work (Brey and Köhler, 1990; Canil and ONeill, 1996; Schumacher, 1991a; Schumacher, 1991b; Taylor, 1998). Thus, the temperature estimations used in this paper are determined assuming that all Fe in pyroxene is Fe^{2+}.

Taylor's (1998) two-pyroxene thermometer yields temperatures from 820 ˚C to 920 ˚C for our samples. These temperature estimates, based on T98, agree to within ±10 ˚C with temperatures estimated using NT and to within ±20 ˚C with temperatures estimated using BK (Table 1). These differences are relatively small, and the agreement between various formulations of the two-pyroxene thermometer argues that the temperatures given on Table 1 are reliable estimates of the temperature of mineral equilibration (± 50 ˚C).

As discussed previously, amphibole grains often occur as rims on spinel or clinopyroxene grains, and some of the mineral grains do exhibit small core to rim chemical variations (Figures 2 and 3). Given these textural relations we have chosen to use rim compositions for all estimates of T, $a H_2O$, and $f O_2$. However, given the relatively small chemical differences between core and rim, substitution of core compositions for rim compositions makes minor differences in estimated temperature and fluid fugacities. For example, the compositions of pyroxene cores from sample GN9912 yields a Taylor (1998) two-pyroxene temperature of 819 ˚C whereas the rim compositions yield a T of 818 ˚C. We report these temperatures to three significant digits for the purposes of comparison only and, given the uncertainties involved, both these temperatures are approximately 820 ˚C.

O'Reilly and Griffin (1985) used the garnet-orthopyroxene barometer of Wood (1974) and the garnet-clinopyroxene thermometer of Ellis and Green (1979) to determine P-T conditions for

This is the peer-reviewed, final accepted version for American Mineralogist, published by the Mineralogical Society of America.
The published version is subject to change. Cite as Authors (Year) Title. American Mineralogist, in press.
DOI: https://doi.org/10.2138/am-2022-8735. http://www.minsocam.org/

311 xenoliths collected from Eastern Australia. These P-T estimates define a geothermal gradient for
312 Eastern Austraila, and we have modified this geothermal gradient to be consistent with our choice
313 of the T98 two-pyroxene thermometer (Taylor, 1998). This modified geotherm yields pressures
314 for the four samples from Eastern Australia that range from 1.1-1.4 GPa (Table 1). The depth of
315 the Moho in Eastern Australia is approximately 32 km (Kennett et al., 2011; Salmon et al., 2013).
316 Therefore, the minimum pressure for these samples is approximately 1.0 GPa, while the maximum
317 pressure, based on the P-T location of the spinel-to-garnet transition (O'Neill, 1981) is
318 approximately 1.9 GPa. Thus, pressure constraints estimated using the geotherm are consistent
319 with both the minimum and maximum pressure estimates based on the depth of the Moho and the
320 spinel-garnet transition, respectively.

321 ## Activities of H_2O

322 Application of H_2O-buffering equilibria to estimate values of aH_2O in samples that contain
323 co-existing olivine, orthopyroxene, clinopyroxene, amphibole, and spinel has been the subject of
324 previous publications (Bonadiman et al., 2014; Gentili et al., 2015; Hunt and Lamb, 2019; Kang
325 et al., 2017; Lamb and Popp, 2009). This study uses an approach similar to that outlined by Lamb
326 and Popp (2009) who chose to use THERMOCALC (Powell et al., 1998; Powell and Holland,
327 1988) largely because of the availability of relatively sophisticated models describing the activity-
328 composition (a-X) relations in amphiboles (Dale et al., 2005; Diener et al., 2007) . Additional a-
329 X models have been published (Palin et al., 2016), including models specifically designed for
330 mantle P-T-X conditions (Holland et al., 2013; Holland et al., 2018; Holland and Powell, 2011;
331 Jennings and Holland, 2015). AX software was applied in this study to determine the activities of
332 end-members in mineral species, although the choice of activity model, has little effect on the

333 value of end-member activities for certain phases, including Mg_2SiO_4 in olivine (Lamb and Popp,
334 2009).

335 Given co-existing olivine, orthopyroxene, clinopyroxene, amphibole, and spinel, several
336 different H_2O-buffering equilibria can be written that involve end-member components in the
337 natural phases. Lamb and Popp (2009), applied the equilibria:

338 2 Pargasite + Enstatite = 2 Forsterite +4 Diopside + 2 Jadeite +2 Spinel + H_2O (1).

339 $2\ NaCa_2Mg_4Al(Al_2Si_6)O_{22}(OH)_2 + Mg_2Si_2O_6 =$

340 $= 2\ Mg_2SiO_4 + 4\ CaMgSi_2O_6 + 2\ NaAlSi_2O_6 + 2\ MgAl_2O_4 + H_2O$

341 which was chosen in large part due to the Mg-rich nature of olivine, orthopyroxenes, and spinel,
342 and the pargasite-rich amphiboles found in these samples (Lamb and Popp, 2009). However, given
343 that pargasite is a reactant, the products must contain the Na-bearing phase, and, therefore, jadeite
344 is included as one of the products. The Na content in the clinopyroxenes, while significant, is not
345 large relative to the concentrations of most of the other end-members included in equilibria 1 (e.g.,
346 the diopside end-member in clinopyroxene or the forsterite end-member in olivine). Thus, the
347 uncertainty in activity of the jadeite end-member may be large relative to that of most other end-
348 members included in equilibrium (1). For example, activities of the diopside end-members in
349 clinopyroxenes analyzed for this study ranging from 0.65 to 0.72 (Table 2), as estimated using the
350 AX software which also yields an uncertainty of 5% in each case (the 2018 version of the AX
351 software, written by T.J.B. Holland, was applied in this study; Diener et al., 2007; Holland et al.,
352 2013; Powell et al., 2014; White et al., 2014). The activities of jadeite end-members in the same
353 clinopyroxenes range from 0.08 to 0.11, with uncertainties ranging from 13% to 16% of the amount
354 present.

355 We report values of aH_2O based on equilibrium (1) in Table 1. We have also estimated
356 values of aH_2O using the equilibria:

This is the peer-reviewed, final accepted version for American Mineralogist, published by the Mineralogical Society of America.
The published version is subject to change. Cite as Authors (Year) Title. American Mineralogist, in press.
DOI: https://doi.org/10.2138/am-2022-8735. http://www.minsocam.org/

357 2 Tremolite + 2 Forsterite = 4 Diopside + 5 Enstatite + 2 H_2O (2)

358 2 $Ca_2Mg_5Si_8O_{22}(OH)_2$ + 2 Mg_2SiO_4 = 4 $CaMgSi_2O_6$ + 5 $Mg_2Si_2O_6$ + 2 H_2O

359

360 which eliminates the need to include the jadeite end-member. However, uncertainties for the
361 tremolite end-members range from 16 to 17% of the amount present for three of our samples
362 (GN9912, GN99113, and BM9912) and 26% for sample BM9915. Whereas the activities of the
363 pargasite end-member, used in equilibrium (1), have uncertainties that range from 12 to 13% of
364 the amount present for all samples.

365 The activities of amphibole end-member species, as determined using AX software, does
366 not consider substitution on the hydroxyl site. Thus, the values determined with AX were modified
367 to account for constituents other than OH on this site (e.g., O and Cl) using an approach similar to
368 that of Popp et al. (2006). Given that maximum and minimum values of the oxy-component were
369 generated for the average compositions of the amphibole in each of the samples analyzed we have
370 determined maximum and minimum values of the activities of the pargasite and tremolite end-
371 members that correspond to the maximum and minimum values of the hydroxyl content,
372 respectively.

373 The activities of mineral end-members (Table 2) were applied when using
374 THERMOCALC to estimate values of $a$$H_2O$ at the P-T conditions given in Table 2. These
375 calculations were performed using THERMOCALC version 3.50β and dataset 6.33 (e.g., Green
376 et al., 2016; Holland et al., 2018). The approach is shown on Figure 4 for sample BM9915 which
377 illustrates the stability of equilibria (1) and (2) at 13 GPa. Although both equilibria ((1) and (2))
378 are shown on the same diagram, we consider them independently (i.e., the diagram does not
379 necessarily obey Schreinemaker's rules). The curves labeled “2a” and “2b” on Figure 4 illustrate
380 the stability of equilibria 2 as a function of T and $a$$H_2O$. Curve 2a (solid) is based on an amphibole

normalization that assumed $Fe^{3+}/\Sigma Fe = 0$, while the dashed line (2b) assumes $Fe^{3+}/\Sigma Fe$ in this amphibole = 1. Values of aH_2O based on equilibria 2 for sample BM9915 fall between 0.08 and 0.13 as shown by the open and closed circles, respectively (Table 2). The curve labeled "1a" (solid) on Figure 4 illustrates the stability of equilibrium (1) for a value of $Fe^{3+}/\Sigma Fe$ in the amphibole = 0, while "1b" (dashed) illustrates the same equilibrium for an amphibole with $Fe^{3+}/\Sigma Fe = 1$. This equilibrium yields values of aH_2O of 0.1 (1a) and 0.06 (1b). Thus, both equilibria 1 and 2 yield similar values of aH_2O with differences between the two estimates less than 0.03 (Figure 4).

Uncertainties in values of aH_2O were estimated for the samples in this study by combining the uncertainty THERMOCALC provides for any given equilibrium (reported in ˚C), with the temperature uncertainty estimated previously (± 50 ˚C). In the case of sample BM9915, the uncertainty for equilibrium (2) yields a maximum value of $aH_2O = 0.27$ (solid hexagon on curve 2a, Figure 4) and a minimum value of $aH_2O = 0.03$ (open hexagon on curve 2b, Figure 4). The temperature uncertainty for equilibrium (1) is approximately ± 350 ˚C. However, given the slope of equilibrium (1), this large temperature range does not translate to a large range in possible values of aH_2O, with a maximum of approximately 0.13 (T ≈ 1260 ˚C), and minimum of approximately 0.03 (T ≈ 560 ˚C). Thus, the maximum value of aH_2O estimated from equilibrium (2), with uncertainty included (i.e., 0.27), is not consistent with maximum value of aH_2O estimated from equilibrium (1). Taking into consideration the results from both equilibria, including the uncertainties, the best estimate for sample BM9915 is, therefore, $aH_2O = 0.09 \pm 0.06$.

Application of this approach, as described in the previous paragraph, was applied to all the samples in this study and the results are summarized on Figure 5. Three of the samples yields similar results, this includes BM9915 (discussed above), GN9912, and GM9913. These three

This is the peer-reviewed, final accepted version for American Mineralogist, published by the Mineralogical Society of America.
The published version is subject to change. Cite as Authors (Year) Title. American Mineralogist, in press.
DOI: https://doi.org/10.2138/am-2022-8735. http://www.minsocam.org/

404 samples yield aH$_2$O = 0.13 to 0.17 for equilibrium (2) and 0.10 to 0.11 for equilibrium (1), for an
405 amphibole with $Fe^{3+}/\Sigma Fe = 0$. If $Fe^{3+}/\Sigma Fe = 1$, then these values of aH$_2$O become 0.08 to 0.1
406 (equilibrium (2)) and 0.06 to 0.07 (equilibrium (1)). The differences in estimates of aH$_2$O, between
407 equilibria (1) and (2), range from 0.04 to 0.06 for these three samples (BM9915, GN9912, and
408 GM9913). Although the uncertainty associated with equilibrium (2) indicates values may be as
409 large as 0.26 to 0.33 for amphiboles with $Fe^{3+}/\Sigma Fe = 0.$, the uncertainties associated with
410 equilibrium (1) indicates values of aH$_2$O < 0.15. Minimum values of aH$_2$O for samples BM9915,
411 GN9912, and GM9913, with amphiboles normalized assuming $Fe^{3+}/\Sigma Fe = 0$, range from 0.06 to
412 0.07 for equilibrium (2) and from 0.04 to 0.07 for equilibrium (1). If the amphiboles in these three
413 samples were normalized assuming $Fe^{3+}/\Sigma Fe = 1$, these minimum values become 0.03 to 0.04 for
414 equilibria 1 and 2, respectively. In summary, dehydration equilibria applied to the three of the
415 four xenoliths in this study (BM9915, GN9912, GN9913) indicate values of aH$_2$O ranging from
416 0.08 to 0.13, with minimum and maximum values, given the estimates of uncertainty, of
417 approximately 0.03 and 0.15, respectively.

418 The value of aH$_2$O, estimated for sample BM9912 using equilibrium (2), ranges from 0.23
419 to 0.38, depending on the oxy-amphibole content (Figure 5), and is somewhat greater than the
420 value estimated for the other three samples (0.08 to 0.17). However, application of equilibrium
421 (1) to this samples yields lower values of aH$_2$O that are consistent with those estimated for the
422 other three samples. This relatively large difference in values of aH$_2$O, estimated for BM9912
423 using two different equilibria, may indicate some resetting has occurred, perhaps with pyroxenes
424 retaining high temperature compositions while the amphibole suffered some minor change in
425 composition during cooling. However, the uncertainties associated with estimates of aH$_2$O for
426 sample BM9912 are larger than those estimated for the other samples consistent with the larger

This is the peer-reviewed, final accepted version for American Mineralogist, published by the Mineralogical Society of America.
The published version is subject to change. Cite as Authors (Year) Title. American Mineralogist, in press.
DOI: https://doi.org/10.2138/am-2022-8735. http://www.minsocam.org/

uncertainties associated with the estimates of the activities of amphibole end-members discussed previously. Given these uncertainties (Figure 5), an aH_2O value of 0.17 could be inferred from equilibrium (2) for sample BM9912. This lower limit approaches the upper limit estimated using equilibrium (1) for this sample (≈0.14), suggesting that sample BM9912 may have equilibrated at higher values of aH_2O as compared to the other three samples.

Values of aH_2O estimated from equilibria (1) and (2) are between 0.03 and 0.15 for all samples except BM9912 which my record aH_2O as high as approximately 0.2. Thus, if a lithostatically pressured fluid phase co-existed with these samples during mineral equilibration, H_2O was not the dominant fluid component.

Oxygen Fugacity

Mineral equilibria have often been applied to estimate values of oxygen fugacity (fO_2) in samples containing co-existing olivine, spinel, and orthopyroxene (Ballhaus et al., 1991; Miller et al., 2016; Wood, 1990a; Woodland et al., 1992). In these samples, values of fO_2 are based on the following equilibria:

$$6 \text{ Fayalite} + O_2 = 3 \text{ Ferrosilite} + 2 \text{ Magnetite} \quad (3)$$

$$6\ Fe_2SiO_4 + O_2 = 3\ Fe_2Si_2O_6 + 2\ Fe_3O_4.$$

Values of fO_2 are also typically reported relative to an oxygen-buffering equilibria, such as the Fayalite-Magnetite-Quartz (FMQ) buffer, which is based on the equilibria:

$$3 \text{ Fayalite} + O_2 = 2 \text{ Magnetite} + 3 \text{ Quartz} \quad (4)$$

$$3\ Fe_2SiO_4 + O_2 = 2\ Fe_3O_4 + 3\ SiO_2$$

Values of log fO_2 for the uppermost mantle, as estimated from mineral equilibria, typically range from $\Delta \text{Log} fO_2$(FMQ) of -3 to +2 (Wood, 1990b; Woodland and Koch, 2003; Woodland et al., 1992).

This is the peer-reviewed, final accepted version for American Mineralogist, published by the Mineralogical Society of America.
The published version is subject to change. Cite as Authors (Year) Title. American Mineralogist, in press.
DOI: https://doi.org/10.2138/am-2022-8735. http://www.minsocam.org/

Using the recent calibration of Miller et al. (2016), the values of fO_2 for all four samples range from $\Delta \mathrm{Log} fO_2$(FMQ) of -1.2 to -0.2 (Table 3). These values of fO_2 are similar to values estimated using the calibration of Bryndzia and Wood (1990), as the largest difference between these two calibrations is < 0.2 (Table 3).

C-O-H Equilibria

In the C-O-H system it is possible to write four independent equilibria that relate the fugacities of six fluid species, H_2O, CO_2, CH_4, H_2, CO, and O_2, and the activity of carbon (French, 1966).

$$C + O_2 \leftrightharpoons CO_2 \qquad k_{eq} = \frac{fCO_2}{aC \times fO_2} \qquad (4)$$

$$C + \frac{1}{2}O_2 \leftrightharpoons CO \qquad k_{eq} = \frac{fCO}{aC \times (fO_2)^{\frac{1}{2}}} \qquad (5)$$

$$H_2 + \frac{1}{2}O_2 \leftrightharpoons H_2O \qquad k_{eq} = \frac{fH_2O}{fH_2 \times (fO_2)^{\frac{1}{2}}} \qquad (6)$$

$$CH_4 + 2O_2 \leftrightharpoons CO_2 + 2H_2O \qquad k_{eq} = \frac{fH_2O^2 x fCO_2}{fCH_4 \times fO_2^2} \qquad (7)$$

Furthermore, if the fluid pressure is equivalent to the sum of the partial pressures of the six fluid species, a fifth equation can be written:

$$P_{Lith} = P_{Fluid} = P_{H_2O} + P_{CO_2} + P_{CH_4} + P_{H_2} + P_{CO} + P_{O_2} \qquad (8)$$

(Lith = Lithostatic). Thus, for a given value of P and T, there are five equations and seven unknowns. The unknows are the fugacities of the six fluid species and the activity of carbon (aC).

In a number of cases, values of fO_2, or any other of the six fluid species listed in equation (8), have been combined with the presence of graphite (which fixes aC = 1) to fix two of these variables and solve for the remaining five (French, 1966; Lamb and Valley, 1984; Lamb and Valley, 1985; Wood et al., 1990). Solving simultaneous equations to calculate fluid speciation in the C-O-H system may suggest that a C-O-H fluid is present. The assumption, often implicit, is

that fluid pressure is equivalent to lithostatic pressure (French, 1966; Frost and McCammon, 2008; Ohmoto and Kerrick, 1977; Wood et al., 1990). However, previous studies indicate that minerals in high-grade rocks may equilibrate in the absence of a separate, lithostatically-pressured, C-O-H fluid phase (Kang et al., 2017; Lamb and Valley, 1984; Lamb and Valley, 1985). In this case, it would be more accurate to to argue that we calculate the fugacites of fluid components rather than fluid species (we continue to use the phrase fluid speciation for the sake of continuity). Even in cases where fluid pressure may not be equivalent to lithostatic pressure, calculation of fluid speciation in the C-O-H systems can provide useful constraints on the nature of fluids in these systems (Kang et al., 2017; Lamb and Valley, 1984; Lamb and Valley, 1985).

A revised version of the software "CalCOH" (Lamb, 1987), which now employs the equation of state for C-O-H fluids published by Zhang and Duan (2009; see also, Ivanov and Alexandrovich, 2021), was used to solve equations (4) through (8) (Lamb and Valley, 1984; Lamb and Valley, 1985). Of our four samples, only the most reducing value of fO_2, which is recorded by sample GN9912, falls within the stability field of graphite. Given the estimated value of fO_2 ($\Delta\log fO_2$ (FMQ) = -1.19) and aH_2O (≈ 0.1) for sample GN9912, then if P_{Fluid} = 1.1 GPa, and aC=1, the maximum possible value of aC, then simultaneous solution of equations 4 through 8 yields a minimum value of aH_2O = 0.63 (Table 3 and Figure 6). In other words, if graphite were present (i.e., aC = 1) at these P-T conditions, along with a lithostatically pressured fluid phase, then this sample would likely have equilibrated under water-rich conditions. However, no graphite was detected in this sample, consistent with an activity of C was less than 1. Reducing the activity of carbon expands the range of oxygen fugacity values over which H_2O is the dominant fluid at the expense of carbon-bearing phases, such as CO_2 and CH_4 (Lamb and Valley, 1984, 1985) as shown on Figure 6. The significant difference between the values of XH_2O estimated from mineral

equilibria (< 0.2) and from C-O-H calculations (> 0.6) can only be reconciled if the pressure of a C-O-H fluid is significantly less than the lithostatic pressure. Rather than fixing $P_{Lith} = P_{Fluid}$, it is possible to determine the maximum value of the fluid pressure by assuming aC =1 given values of fO_2 and aH_2O. For sample GN9912 ($\Delta \log fO_2$ (FMQ) = -1.19 and $aH_2O \approx 0.1$) the maximum fluid pressure is approximately 0.55 GPa, which is significantly less than 1.1 GPa, the estimated value of P_{Lith}. This result indicates the absence of a lithostatically-pressured C-O-H fluid phase, although it does not rule out a fluid with additional components.

It may seem counter-intuitive to estimate values of fO_2 and fH_2O, apply equilibria in the C-O-H fluid system, and then suggest that the mineral equilibrated in the absence of a free fluid phase. However, values of fO_2 and fH_2O, as estimated in this study, are measures of chemical potential and do not require the presence of a free fluid phase. In the case of sample GN9912 attempts to apply C-O-H equilibria yield inconsistencies that can be explained if a C-O-H fluid was not present during mineral equilibration (see also, Kang et al., 2017; Lamb and Valley, 1984; Lamb and Valley, 1985). This result suggests that any component typically associated with fluids, such as H_2, is contained within mineral phases (Hunt and Lamb, 2019; Kang et al., 2017; Lamb and Valley, 1984; Lamb and Valley, 1985).

The samples BM9912, BM9915, and GN9913 record values of fO_2 that are more oxidizing than sample GN9912 and fall outside of the stability of graphite. The C-O-H system calculations described above may be used to demonstrate that the values of fO_2 estimated for these three samples rule out the presence of a CH_4-rich fluid in these samples, while CO_2-rich, H_2O-rich, or fluid-absent conditions are all consistent with these values of fO_2. Thus, relatively oxidizing conditions are consistent with, but do not require, the presence of a fluid, including a CO_2-rich fluid.

518 # Discussion

519 Amphibole-bearing peridotite xenoliths from southeastern Australia record estimated
520 values of $a\mathrm{H_2O}$ of 0.2 or less. These low values of $a\mathrm{H_2O}$ are generally consistent with previous
521 estimates that were also based on amphibole equilibria (Bonadiman et al., 2014; Gentili et al.,
522 2015; Hunt and Lamb, 2019; Kang et al., 2017; Lamb and Popp, 2009; Popp et al., 2006), however,
523 application of equilibria involving amphiboles to infer values of intensive parameters in the mantle
524 requires that amphibole compositions do not change during their trip from the mantle to the surface
525 of the Earth. Certain early studies of mantle amphiboles suggest that these minerals may not be
526 reliable indicators of mantle conditions because retrograde H loss may be common (Dyar et al.,
527 1992; Popp et al., 1990). However, more recent studies have supported the conclusion that the
528 compositions of many mantle-derived amphiboles do reflect the original conditions of formation,
529 or if they do not, it may be possible to identify those that have undergone alteration. Information
530 in these studies comes from examination of: (1) diffusion rates of H in amphibole (Dyar et al.,
531 1993), (2) estimates of $a\mathrm{H_2O}$ in the mantle (Popp et al., 1995b), (3) the compositions of mantle
532 amphiboles (King et al., 1999), and (4) the δD values of mantle amphiboles (Boettcher and O'Neil,
533 1980; Deloule et al., 1991; Wagner et al., 1996). Furthermore, Hunt and Lamb (2019)
534 demonstrated that values of $a\mathrm{H_2O}$ estimated from dehydration equilibria are not sensitive to the
535 maximum H loss that could be inferred from analyses of certain amphiboles contained in mantle
536 xenoliths. These authors also demonstrated that values of $a\mathrm{H_2O}$ estimated from dehydration
537 equilibria are in good agreement with values of $a\mathrm{H_2O}$ estimated from a combination of hydrogen
538 fugacities, as estimated from amphibole dehydrogenation equilibria, and oxygen fugacities, as
539 determined using oxybarometry (Hunt and Lamb, 2019). This agreement is strong evidence that
540 application of amphibole equilibria can provide reliable estimates of mantle $a\mathrm{H_2O}$.

The presence of a hydrous phase is consistent with elevated whole-rock water contents, yet these amphibole-bearing samples record values of aH2O < 0.3. Of course, consideration of mixed volatile equilibria demonstrates that hydrous phases do not require H_2O-rich fluids and, therefore, amphibole can be stable at low values of aH_2O (Kerrick, 1974). Furthermore, phase equilibria involving hydrous phases, particularly amphiboles and micas, is one line of evidence indicating that granulite facies metamorphism is characterized by low values of aH_2O (Bader et al., 2014; Edwards and Essene, 1988; Lamb and Valley, 1988; Phillips, 1980; Valley et al., 1990). Previous studies indicate that there is no positive correlation between NAM H_2O contents and the presence of amphiboles in mantle samples (Demouchy and Bolfan-Casanova, 2016; Marshall et al., 2018), a further indication that this phase does not require elevated values of aH_2O. The absence of a positive correlation between the presence of amphibole and the water content of NAMs, and the possibility of a negative correlation (although data are limited), indicates that a portion of the OH in mantle amphiboles could, in some cases, be sourced from co-existing NAMS (Chin et al., 2016; Demouchy and Bolfan-Casanova, 2016; Kang et al., 2017).

It has been argued that the upper 100 km of the earth's mantle is characterized by the presence of a lithostatically pressured CO_2-rich grain boundary fluids (Frezzotti and Touret, 2014). Low values of aH_2O may be consistent with the presence of CO_2-rich fluids. However, one of our samples (GN9912) equilibrated at a value of fO_2 that is not consistent with the presence of a fluid rich in CO_2. No carbon-bearing phase has yet been detected in the other three samples and, therefore, there is no evidence that a CO_2-rich fluid was present, although this possibility cannot be ruled out for samples BM9912, BM9915, and GN9913.

In addition to the sample that records a $\Delta\log fO_2$(FMQ) value of -1.2 (GN9912), the other three samples equilibrated at values of fO_2 that are within 0.4 log units of the FMQ oxygen buffer.

This is the peer-reviewed, final accepted version for American Mineralogist, published by the Mineralogical Society of America.
The published version is subject to change. Cite as Authors (Year) Title. American Mineralogist, in press.
DOI: https://doi.org/10.2138/am-2022-8735. http://www.minsocam.org/

This result, values of fO_2 ≈ FMQ or less, may seem unexpected because mantle amphiboles typically contain significant Fe^{3+}, and it might be argued that elevated values of Fe^{3+} are indicative of relatively oxidizing conditions (Dyar et al., 1993). Bryndzia and Wood (1990), for example, report that amphibole-bearing samples are relatively oxidizing with values of $\Delta\log fO_2$(FMQ) for that range from ~0 to +1.5. Although these values of oxygen fugacity are more oxidizing than FMQ, they do fall within the range of samples that do not contain amphibole ($\Delta\log fO_2$(FMQ) from - 1.5 to 2.0). Furthermore, recent studies have reported values of fO_2 for amphibole-bearing mantle rocks that are significantly below the FMQ oxygen buffer (Bonadiman et al., 2021; Bonadiman et al., 2014; Gentili et al., 2015; Hunt and Lamb, 2019).

Implications

In many instances, a strong case can be made that amphiboles in mantle peridotites form as the result of metasomatism (O'Reilly and Griffin, 2013), including the amphiboles contained in lherzolite xenoliths from the Bullenmerri and Gnotuk Maars (Griffin et al., 1988; O'Reilly and Griffin, 1988). Mantle amphiboles are typically kaersutitic or pargasitic, and are often characterized by relatively elevated Fe^{3+} contents and low H contents (Popp and Bryndzia, 1992). This combination, a hydrous phase with elevated values of Fe^{3+}, might suggest relatively oxidizing conditions along with elevated values of aH_2O (see the previous discussion). Thus, elevated values of both fH_2O and fO_2 could be consistent the presence of oxy-amphiboles. However, if amphibole-bearing mantle peridotites equilibrated over a range of fO_2 values, then a range in H_2O activities might be expected. Furthermore, if the value of fO_2 is approximately FMQ or less, then mantle amphibole will generally record values of aH_2O that are less than 0.5 (Popp et al., 1995b).

Amphibole formation via metasomatism could indicate that infiltrating melts are the source of the water now contained in the amphiboles. Although this may be likely, crystallization of

This is the peer-reviewed, final accepted version for American Mineralogist, published by the Mineralogical Society of America.
The published version is subject to change. Cite as Authors (Year) Title. American Mineralogist, in press.
DOI: https://doi.org/10.2138/am-2022-8735. http://www.minsocam.org/

588 mantle amphiboles may also require the addition of other components, including, but not limited
589 to, alkali elements, Ti, Al, and Fe. These components, if added in sufficient amounts, could be
590 sufficient to stabilize an oxy-amphibole even if no water is added. In this end-member case,
591 however unlikely, the amphibole might act to consume any available water, and the minerals in
592 these rocks may well equilibrate at reduced values of $a\mathrm{H_2O}$. Even if the metasomatic fluid does
593 contain some water, as seems likely, an H-deficient amphibole (i.e., an oxy-amphibole) may
594 crystallize and can be stable at values of $a\mathrm{H_2O}$ that are significantly less than one (Popp et al.,
595 1995b). In this case, the amphibole may scavenge additional water from the NAMs (Chin et al.,
596 2016; Hunt and Lamb, 2019; Kang et al., 2017), record values of $a\mathrm{H_2O} < 1$, and co-exist with
597 NAMs that are not water saturated.

598 It is possible to use values of $a\mathrm{H_2O}$ to estimate the $\mathrm{H_2O}$-content of co-existing olivine using
599 existing calibrations (Gaetani et al., 2014; Mosenfelder et al., 2006; Padron-Navarta and Hermann,
600 2017; Zhao et al., 2004). For example, the calibration of Mosenfelder et al. (2006) yields on olivine
601 $\mathrm{H_2O}$ content of 10 to 21 ppm by weight for sample BM9915 (with $a\mathrm{H_2O} \approx 0.06$ to 0.13). Although
602 such calibrations will likely be modified as more information becomes available (Tollan et al.,
603 2017), these results indicate that the olivine in the samples analyzed for this study should have low
604 water contents relative to other many other mantle olivines (Chin and Palin, 2022; Demouchy and
605 Bolfan-Casanova, 2016; Peslier et al., 2017).

606 Portions of the earth's mantle that have been metasomatized, including regions that have
607 experienced the passage of melts, may be amphibole-bearing (e.g., O'Reilly and Griffin, 2013).
608 These amphibole-bearing regions of the mantle, which could persist after the igneous episode, may
609 be characterized by relatively low values of $a\mathrm{H_2O}$, and, therefore, high viscosities. However, many
610 mantle xenoliths, including some that exhibit evidence of metasomatism, do not contain amphibole

611 (O'Reilly and Griffin, 2013). Thus, amphibole may be produced locally and contribute to the
612 mantle heterogeneity with respect to water content of NAMs and the physical properties that
613 depend, to some extent, on this water content (e.g., viscosity).

614

615 **Acknowledgements:** Comments provided by David Dojles, Emily Chin, and two anonymous
616 reviewers improved this manuscript. Ayoti Ghosh assisted with sample procurement, and we
617 thank Suzanne O'Reilly for providing the samples examined in this study. Ray Guillemette
618 assisted with electron microprobe analyses.

619

620 **References**
621
622 Asimow, P.D., and Langmuir, C.H. (2003) The importance of water to oceanic mantle melting
623 regimes. Nature, 421(6925), 815-820.

624 Bader, T., Franz, L., De Capitani, C., and Zhang, L.F. (2014) The effect of water activity on
625 calculated phase equilibria and garnet isopleth thermobarometry of granulites, with
626 particular reference to Tongbai (east-central China). European Journal of Mineralogy,
627 26(1), 5-23.

628 Ballhaus, C., Berry, R.F., and Green, D.H. (1991) High-Pressure Experimental Calibration of the
629 Olivine-Ortho-Pyroxene-Spinel Oxygen Geobarometer - Implications for the Oxidation-
630 State of the Upper Mantle. Contributions to Mineralogy and Petrology, 107(1), 27-40.

631 Bell, D.R., and Rossman, G.R. (1992) Water in earth's mantle- The role of nominally anhydrous
632 minerals. Science, 255(5050), 1391-1397.

633 Beran, A., and Libowitzky, E. (2006) Water in natural mantle minerals II: Olivine, garnet and
634 accesssory minerals. In H. Keppler, and J.R. Smyth, Eds. Water in Nominally Anhydrous
635 MInerals, 62, p. 155-167. Mineralogical Society of America.

636 Black, B.A., and Gibson, S.A. (2019) Deep Carbon and the Life Cycle of Large Igneous
637 Provinces. Elements, 15(5), 319-324.

638 Blundy, J.D., Brodholt, J.P., and Wood, B.J. (1991) Carbon Fluid Equilibria and the Oxidation-
639 State of the Upper Mantle. Nature, 349(6307), 321-324.

640 Boettcher, A.L., and O'Neil, J.R. (1980) Stable Isotope, Chemical, and Petrographic Studies of
641 High-Pressure Amphiboles and Micas - Evidence for Metasomatism in the Mantle Source
642 Regions of Alkali Basalts and Kimberlites. American Journal of Science, 280, 594-621.

643 Bolfan-Casanova, N. (2005) Water in the Earth's mantle. Mineralogical Magazine, 69(3), 229-
644 258.

645 Bonadiman, C., Brombin, V., Andreozzi, G.B., Benna, P., Coltorti, M., Curetti, N., Faccini, B.,
646 Merli, M., Pelorosso, B., Stagno, V., Tesauro, M., and Pavese, A. (2021) Phlogopite-
647 pargasite coexistence in an oxygen reduced spinel-peridotite ambient. Scientific Reports,
648 11(1).

649 Bonadiman, C., Nazzareni, S., Coltorti, M., Comodi, P., Giuli, G., and Faccini, B. (2014) Crystal
650 chemistry of amphiboles: implications for oxygen fugacity and water activity in
651 lithospheric mantle beneath Victoria Land, Antarctica. Contributions to Mineralogy and
652 Petrology, 167(3).

Brey, G.P., and Köhler, T. (1990) Geothermobarometry in Four-phase Lherzolites II. New Thermobarometers, and Practical Assessment of Existing Thermobarometers. Journal of Petrology, 31(6), 1353-1378.

Bryndzia, L.T., and Wood, B.J. (1990) Oxygen Thermobarometry of Abyssal Spinel Peridotites - the Redox State and C-O-H Volatile Composition of the Earths Sub-Oceanic Upper Mantle. American Journal of Science, 290(10), 1093-1116.

Canil, D., and ONeill, H.S.C. (1996) Distribution of ferric iron in some upper-mantle assemblages. Journal of Petrology, 37(3), 609-635.

Chin, E.J., and Palin, R.M. (2022) Water storage in cratonic mantle. Terra Nova, 34(5), 369-380.

Chin, E.J., Soustelle, V., Hirth, G., Saal, A.E., Kruckenberg, S.C., and Eiler, J.M. (2016) Microstructural and geochemical constraints on the evolution of deep arc lithosphere. Geochemistry Geophysics Geosystems, 17(7), 2497-2521.

Chu, X., and Ague, J.J. (2013) Phase equilibria for graphitic metapelite including solution of CO2 in melt and cordierite: implications for dehydration, partial melting and graphite precipitation. Journal of Metamorphic Geology, 31(8), 843-862.

Connolly, J.A.D., and Cesare, B. (1993) C-O-H-S Fluid Composition and Oxygen Fugacity in Graphitic Metapelites. Journal of Metamorphic Geology, 11(3), 379-388.

Dale, J., Powell, R., White, R.W., Elmer, F.L., and Holland, T.J.B. (2005) A thermodynamic model for Ca-Na clinoamphiboles in Na_2O-CaO-FeO-MgO-Al_2O_3-SiO_2-H_2O-O for petrological calculations. Journal of Metamorphic Geology, 23(8), 771-791.

Dasgupta, R., and Hirschmann, M.M. (2010) The deep carbon cycle and melting in Earth's interior. Earth and Planetary Science Letters, 298(1-2), 1-13.

Deloule, E., Albarede, F., and Sheppard, S.M.F. (1991) Hydrogen Isotope Heterogeneities in the Mantle from Ion Probe Analysis of Amphiboles from Ultramafic Rocks. Earth and Planetary Science Letters, 105(4), 543-553.

Demouchy, S., and Bolfan-Casanova, N. (2016) Distribution and transport of hydrogen in the lithospheric mantle: A review. Lithos, 240, 402-425.

Demouchy, S., Tommasi, A., Barou, F., Mainprice, D., and Cordier, P. (2012) Deformation of olivine in torsion under hydrous conditions. Physics of the Earth and Planetary Interiors, 202, 56-70.

683 Diener, J.F.A., Powell, R., White, R.W., and Holland, T.J.B. (2007) A new thermodynamic
684 model for clino- and orthoamphiboles in the system Na_2O-CaO-FeO-MgO-Al_2O_3-SiO_2-
685 H_2O-O. Journal of Metamorphic Geology, 25(6), 631-656.

686 Dyar, M.D., Mackwell, S.J., McGuire, A.V., Cross, L.R., and Robinson, J.D. (1993) Crystal
687 chemistry of Fe^{3+} and H^+ in mantle kaersutite-Implications for mantle metasomatism.
688 American Mineralogist, 78, 968-979.

689 Dyar, M.D., Mcguire, A.V., and Mackwell, S.J. (1992) Fe^{3+}/H^+ and D/H in Kaersutites -
690 Misleading Indicators of Mantle Source Fugacities. Geology, 20(6), 565-568.

691 Dyar, M.D., Mcguire, A.V., and Ziegler, R.D. (1989) Redox Equilibria and Crystal-Chemistry of
692 Coexisting Minerals from Spinel Iherzolite Mantle Xenoliths. American Mineralogist,
693 74(9-10), 969-980.

694 Edwards, R.L., and Essene, E.J. (1988) Pressure, Temperature and C-O-H Fluid Fugacities
695 across the Amphibolite Granulite Transition, Northwest Adirondack Mountains, New-
696 York. Journal of Petrology, 29(1), 39-72.

697 Ejima, T., Osanai, Y., Akasaka, M., Adachi, T., Nakano, N., Kon, Y., Ohfuji, H., and Sereenen,
698 J. (2018) Oxidation States of Fe in Constituent Minerals of a Spinel Lherzolite Xenolith
699 from the Tariat Depression, Mongolia: The Significance of Fe^{3+} in Olivine. Minerals,
700 8(5).

701 Ellis, D.J., and Green, D.H. (1979) Experimental-Study of the Effect of Ca Upon Garnet-
702 Clinopyroxene Fe-Mg Exchange Equilibria. Contributions to Mineralogy and Petrology,
703 71(1), 13-22.

704 Faul, U.H., Cline, C.J., David, E.C., Berry, A.J., and Jackson, I. (2016) Titanium-hydroxyl
705 defect-controlled rheology of the Earth's upper mantle. Earth and Planetary Science
706 Letters, 452, 227-237.

707 French, B.M. (1966) Some Geological Implications of Equilibrium between Graphite and a C -
708 H - O Gas Phase at High Temperatures and Pressures. Reviews of Geophysics, 4(2), 223-
709 253.

710 Frezzotti, M.L., and Touret, J.L.R. (2014) CO2, carbonate-rich melts, and brines in the mantle.
711 Geoscience Frontiers, 5(5), 697-710.

712 Frost, D.J., and McCammon, C.A. (2008) The Redox State of Earth's Mantle. Annual Review of
713 Earth and Planetary Sciences, 36(1), 389-420.

714 Gaetani, G.A., and Grove, T.L. (1998) The influence of water on melting of mantle peridotite.
715 Contributions to Mineralogy and Petrology, 131(4), 323-346.

716 Gaetani, G.A., O'Leary, J.A., Koga, K.T., Hauri, E.H., Rose-Koga, E.F., and Monteleone, B.D.
717 (2014) Hydration of mantle olivine under variable water and oxygen fugacity conditions.
718 Contributions to Mineralogy and Petrology, 167(2), 1-14.

719 Gentili, S., Bonadiman, C., Biagioni, C., Comodi, P., Coltorti, M., Zucchini, A., and Ottolini, L.
720 (2015) Oxo-amphiboles in mantle xenoliths: evidence for H2O-rich melt interacting with
721 the lithospheric mantle of Harrow Peaks (Northern Victoria Land, Antarctica).
722 Mineralogy and Petrology, 109(6), 741-759.

723 Ghent, E.D., Edwards, B.R., and Russell, J.K. (2019) Pargasite-bearing vein in spinel lherzolite
724 from the mantle lithosphere of the North America Cordillera. Canadian Journal of Earth
725 Sciences, 56(8), 870-885.

726 Gibson, S.A., Rooks, E.E., Day, J.A., Petrone, C.M., and Leat, P.T. (2020) The role of sub-
727 continental mantle as both "sink" and "source" in deep Earth volatile cycles. Geochimica
728 Et Cosmochimica Acta, 275, 140-162.

729 Girard, J., Chen, J.H., Raterron, P., and Holyoke, C.W. (2013) Hydrolytic weakening of olivine
730 at mantle pressure: Evidence of [100](010) slip system softening from single-crystal
731 deformation experiments. Physics of the Earth and Planetary Interiors, 216, 12-20.

732 Goncharov, A.G., Ionov, D.A., Doucet, L.S., and Pokhilenko, L.N. (2012) Thermal state, oxygen
733 fugacity and C-O-H fluid speciation in cratonic lithospheric mantle: New data on
734 peridotite xenoliths from the Udachnaya kimberlite, Siberia. Earth and Planetary Science
735 Letters, 357, 99-110.

736 Green, D.H. (2015) Experimental petrology of peridotites, including effects of water and carbon
737 on melting in the Earth's upper mantle. Physics and Chemistry of Minerals, 42(2), 95-
738 122.

739 Green, D.H., Hibberson, W.O., Rosenthal, A., Kovacs, I., Yaxley, G.M., Falloon, T.J., and
740 Brink, F. (2014) Experimental Study of the Influence of Water on Melting and Phase
741 Assemblages in the Upper Mantle. Journal of Petrology, 55(10), 2067-2096.

742 Green, E.C.R., White, R.W., Diener, J.F.A., Powell, R., Holland, T.J.B., and Palin, R.M. (2016)
743 Activity-composition relations for the calculation of partial melting equilibria in
744 metabasic rocks. Journal of Metamorphic Geology, 34(9), 845-869.

745 Griffin, W.L., Oreilly, S.Y., and Stabel, A. (1988) Mantle Metasomatism beneath Western
746 Victoria, Australia .2. Isotopic Geochemistry of Cr-Diopside Iherzolites and Al-Augite
747 Pyroxenites. Geochimica Et Cosmochimica Acta, 52(2), 449-459.

748 Griffin, W.L., Wass, S.Y., and Hollis, J.D. (1984) Ultramafic xenoliths from Bullen Merri and
749 Gnotuk Maars, Victoria, Australia: Petrology of a sub-continental crust-mantle transition.
750 Journal of Petrology, 25, 53-87.

751 Hazen, R.M., and Schiffries, C.M. (2013) Why Deep Carbon? Carbon in Earth, 75, 1-6.

752 Hirschmann, M.M. (2006) Water, melting, and the deep Earth H2O cycle. Annual Review of
753 Earth and Planetary Sciences, 34, 629-653.

754 Holland, T.J., Hudson, N.F., Powell, R., and Harte, B. (2013) New Thermodynamic Models and
755 Calculated Phase Equilibria in NCFMAS for Basic and Ultrabasic Compositions through
756 the Transition Zone into the Uppermost Lower Mantle. Journal of Petrology, 54(9), 1901-
757 1920.

758 Holland, T.J.B., Green, E.C.R., and Powell, R. (2018) Melting of Peridotites through to Granites:
759 A Simple Thermodynamic Model in the System KNCFMASHTOCr. Journal of
760 Petrology, 59(5), 881-899.

761 Holland, T.J.B., and Powell, R. (2011) An improved and extended internally consistent
762 thermodynamic dataset for phases of petrological interest, involving a new equation of
763 state for solids. Journal of Metamorphic Geology, 29(3), 333-383.

764 Howell, D., Stachel, T., Stern, R.A., Pearson, D.G., Nestola, F., Hardman, M.F., Harris, J.W.,
765 Jaques, A.L., Shirey, S.B., Cartigny, P., Smit, K.V., Aulbach, S., Brenker, F.E., Jacob,
766 D.E., Thomassot, E., Walter, M.J., and Navon, O. (2020) Deep carbon through time:
767 Earth's diamond record and its implications for carbon cycling and fluid speciation in the
768 mantle. Geochimica Et Cosmochimica Acta, 275, 99-122.

769 Hunt, L.E., and Lamb, W.M. (2019) Application of mineral equilibria to estimate fugacities of
770 H_2O, H_2, and O_2 in mantle xenoliths from the southwestern USA. American Mineralogist,
771 104(3), 333-347.

772 Ingrin, J., and Skogby, H. (2000) Hydrogen in nominally anhydrous upper-mantle minerals
773 concentration levels and implications. European Journal of Mineralogy, 12(3), 543-570.

774 Ionov, D.A., and Wood, B.J. (1992) The oxidation state of subcontinental mantle: oxygen
775 thermobarometry of mantle xenoliths from central Asia. Contributions to Mineralogy and
776 Petrology, 111(2), 179-193.

Ivanov, M.V., and Alexandrovich, O.V. (2021) Phase State and Thermodynamic Parameters of the Fluid System H
O-CO
-CH
at
Conditions of the Crust and Lithosphere Mantle. Petrology, 29(4), 439-447.

Jennings, E.S., and Holland, T.J.B. (2015) A Simple Thermodynamic Model for Melting of Peridotite in the System NCFMASOCr. Journal of Petrology, 56(5), 869-892.

Jung, H., Katayama, I., Jiang, Z., Hiraga, I., and Karato, S. (2006) Effect of water and stress on the lattice-preferred orientation of olivine. Tectonophysics, 421(1-2), 1-22.

Kang, P., Lamb, W.M., and Drury, M. (2017) Using mineral equilibria to estimate H_2O activities in peridotites from the Western Gneiss Region of Norway. American Mineralogist, 102(5), 1021-1036.

Karato, S. (2019) Some remarks on hydrogen-assisted electrical conductivity in olivine and other minerals. Progress in Earth and Planetary Science, 6(1).

Karato, S., and Jung, H. (1998) Water, partial melting and the origin of the seismic low velocity and high attenuation zone in the upper mantle. Earth and Planetary Science Letters, 157, 193-207.

Karlsen, K.S., Conrad, C.P., and Magni, V. (2019) Deep Water Cycling and Sea Level Change Since the Breakup of Pangea. Geochemistry Geophysics Geosystems, 20(6), 2919-2935.

Kelemen, P.B., and Manning, C.E. (2015) Reevaluating carbon fluxes in subduction zones, what goes down, mostly comes up. Proceedings of the National Academy of Sciences of the United States of America, 112(30), E3997-E4006.

Kennett, B.L.N., Salmon, M., Saygin, E., and Grp, A.W. (2011) AusMoho: the variation of Moho depth in Australia. Geophysical Journal International, 187(2), 946-958.

Kerrick, D.M. (1974) Review of Metamorphic Mixed-Volatile (H_2O-CO_2) Equilibria. American Mineralogist, 59(7-8), 729-762.

King, P.L., Hervig, R.L., Holloway, J.R., Vennemann, T.W., and Righter, K. (1999) Oxy-substitution and dehydrogenation in mantle-derived amphibole megacrysts. Geochimica et Cosmochimica Acta, 63, 3635-3651.

807 Korenaga, J., Planavsky, N.J., and Evans, D.A.D. (2017) Global water cycle and the coevolution
808 of the Earth's interior and surface environment. Philosophical Transactions of the Royal
809 Society a-Mathematical Physical and Engineering Sciences, 375(2094).

810 Kovacs, I.J., Liptai, N., Koptev, A., Cloetingh, S.A.P.L., Lange, T.P., Matenco, L., Szakacs, A.,
811 Radulian, M., Berkesi, M., Patko, L., Molnar, G., Novak, A., Wesztergom, V., Szabo, C.,
812 and Fancsik, T. (2021) The 'pargasosphere' hypothesis: Looking at global plate tectonics
813 from a new perspective. Global and Planetary Change, 204.

814 Lamb, W.M. (1987) Metamorphic fluids and granulite genesis. Geology & Geophysics, Ph.D., p.
815 234. University of Wisconsin.

816 Lamb, W.M., Guillemette, R., Popp, R.K., Fritz, S.J., and Chmiel, G.J. (2012) Determination of
817 Fe3+/Fe using the electron microprobe: A calibration for amphiboles. American
818 Mineralogist, 97(5-6), 951-961.

819 Lamb, W.M., and Popp, R.K. (2009) Amphibole equilibria in mantle rocks: Determining values
820 of mantle aH_2O and implications for mantle H_2O contents. American Mineralogist, 94(1),
821 41-52.

822 Lamb, W.M., and Valley, J.W. (1984) Metamorphism of Reduced Granulites in Low-CO_2
823 Vapor-Free Environment. Nature, 312(5989), 56-58.

824 Lamb, W.M., and Valley, J.W. (1985) C-O-H fluid calculations and granulite genesis. In A.
825 Tobi, and J. Touret, Eds. The deep proterozoic crust in the North Atlantic Provinces, p.
826 119-131. Reidel Pub.

827 -. (1988) Granulite Facies Amphibole and Biotite Equilibria, and Calculated Peak-Metamorphic
828 Water Activities. Contributions to Mineralogy and Petrology, 100(3), 349-360.

829 Marshall, E.W., Lassiter, J.C., and Barnes, J.D. (2018) On the (mis)behavior of water in the
830 mantle: Controls on nominally anhydrous mineral water content in mantle peridotites.
831 Earth and Planetary Science Letters, 499, 219-229.

832 Masuti, S., Karato, S., Girard, J., and Barbot, S.D. (2019) Anisotropic high-temperature creep in
833 hydrous olivine single crystals and its geodynamic implications. Physics of the Earth and
834 Planetary Interiors, 290, 1-9.

835 Mei, S., and Kohlstedt, D.L. (2000a) Influence of water on plastic deformation of olivine
836 aggregates: 1. Diffusion creep regime. Journal of Geophysical Research, 105(B9), 21457-
837 21469.

-. (2000b) Influence of water on plastic deformation of olivine aggregates: 2. Dislocation creep regime. Journal of Geophysical Research, 105(B9), 21471-21481.

Mierdel, K., and Keppler, H. (2004) The temperature dependence of water solubility in enstatite. Contributions to Mineralogy and Petrology, 148(3), 305-311.

Mierdel, K., Keppler, H., Smyth, J.R., and Langenhorst, F. (2007) Water solubility in aluminous orthopyroxene and the origin of Earth's asthenosphere. Science, 315(5810), 364-368.

Miller, W.G.R., Holland, T.J.B., and Gibson, S.A. (2016) Garnet and Spinel Oxybarometers: New Internally Consistent Multi-equilibria Models with Applications to the Oxidation State of the Lithospheric Mantle. Journal of Petrology, 57(6), 1199-1222.

Mosenfelder, J.L., Deligne, N.I., Asimow, P.D., and Rossman, G.R. (2006) Hydrogen incorporation in olivine from 2–12 GPa. American Mineralogist, 91(2-3), 285-294.

Niida, K., and Green, D.H. (1999) Stability and chemical composition of pargasitic amphibole in MORB pyrolite under upper mantle conditions. Contributions to Mineralogy and Petrology, 135(1), 18-40.

Nimis, P., and Grutter, H. (2010) Internally consistent geothermometers for garnet peridotites and pyroxenites. Contributions to Mineralogy and Petrology, 159(3), 411-427.

Nimis, P., and Taylor, W.R. (2000) Single clinopyroxene thermobarometry for garnet peridotites. Part I. Calibration and testing of a Cr-in-Cpx barometer and an enstatite-in-Cpx thermometer. Contributions to Mineralogy and Petrology, 139(5), 541-554.

O'Neill, H.S.C. (1981) The Transition between Spinel Lherzolite and Garnet Lherzolite, and Its Use as a Geobarometer. Contributions to Mineralogy and Petrology, 77(2), 185-194.

O'Reilly, S.Y., and Griffin, W.L. (1987) Eastern Australia - 4000 kilometers of mantle samples. In P.H. Nixon, Ed. Mantle Xenoliths, p. 267-280. John Wiley & Sons Ltd.

-. (2013) Mantle Metasomatism. In D.E. Harlov, and H. Austrheim, Eds. Metasomatism and the Chemical Transformation of Rock, 471-533. Springer, Berlin.

O'Reilly, S.Y., and Griffin, W.L. (1985) A Xenolith-Derived Geotherm for Southeastern Australia and Its Geophysical Implications. Tectonophysics, 111(1-2), 41-63.

-. (1988) Mantle Metasomatism beneath Western Victoria, Australia .1. Metasomatic Processes in Cr-Diopside Lherzolites. Geochimica Et Cosmochimica Acta, 52(2), 433-447.

867 Ohmoto, H., and Kerrick, D. (1977) Devolatilization Equilibria in Graphitic Systems. American
868 Journal of Science, 277(8), 1013-1044.

869 Padron-Navarta, J.A., and Hermann, J. (2017) A Subsolidus Olivine Water Solubility Equation
870 for the Earth's Upper Mantle. Journal of Geophysical Research-Solid Earth, 122(12),
871 9862-9880.

872 Palin, R.M., White, R.W., Green, E.C.R., Diener, J.F.A., Powell, R., and Holland, T.J.B. (2016)
873 High-grade metamorphism and partial melting of basic and intermediate rocks. Journal of
874 Metamorphic Geology, 34(9), 871-892.

875 Peslier, A.H. (2010) A review of water contents of nominally anhydrous natural minerals in the
876 mantles of Earth, Mars and the Moon. Journal of Volcanology and Geothermal Research,
877 197(1-4), 239-258.

878 Peslier, A.H., Schonbachler, M., Busemann, H., and Karato, S.I. (2017) Water in the Earth's
879 Interior: Distribution and Origin. Space Science Reviews, 212(1-2), 743-810.

880 Peslier, A.H., Woodland, A.B., Bell, D.R., and Lazarov, M. (2010) Olivine water contents in the
881 continental lithosphere and the longevity of cratons. Nature, 467(7311), 78-U108.

882 Phillips, G.N. (1980) Water Activity Changes across an Amphibolite-Granulite Facies
883 Transition, Broken-Hill, Australia. Contributions to Mineralogy and Petrology, 75(4),
884 377-386.

885 Popp, R.K., and Bryndzia, L.T. (1992) Statistical-Analysis of Fe^{3+}, Ti, and OH in Kaersutite
886 from Alkalic Igneous Rocks and Mafic Mantle Xenoliths. American Mineralogist, 77(11-
887 12), 1250-1257.

888 Popp, R.K., Hibbert, H.A., and Lamb, W.M. (2006) Oxy-amphibole equilibria in Ti-bearing
889 calcic amphiboles: Experimental investigation and petrologic implications for mantle-
890 derived amphiboles. American Mineralogist, 91(1), 54-66.

891 Popp, R.K., Phillips, M.W., and Harrell, J.A. (1990) Accommodation of Fe^{3+} in Natural, Fe^{3+}-
892 Rich, Calcic and Subcalcic Amphiboles - Evidence from Published Chemical-Analyses.
893 American Mineralogist, 75(1-2), 163-169.

894 Popp, R.K., Virgo, D., and Phillips, M.W. (1995a) H deficiency in kaersutitic amphiboles:
895 Experimental verification. American Mineralogist, 80(11), 1347-1350.

896 Popp, R.K., Virgo, D., Yoder, H.S., Hoering, T.C., and Phillips, M.W. (1995b) An
897 Experimental-Study of Phase-Equilibria and Fe Oxy-Component in Kaersutitic

Amphibole - Implications for the (fH_2) and a(H_2O) in the Upper-Mantle. American Mineralogist, 80(5-6), 534-548.

Powell, R., Holland, T., and Worley, B. (1998) Calculating phase diagrams involving solid solutions via non-linear equations, with examples using THERMOCALC. Journal of Metamorphic Geology, 16(4), 577-588.

Powell, R., and Holland, T.J.B. (1988) An Internally Consistent Dataset with Uncertainties and Correlations .3. Applications to Geobarometry, Worked Examples and a Computer-Program. Journal of Metamorphic Geology, 6(2), 173-204.

Powell, R., White, R.W., Green, E.C.R., Holland, T.J.B., and Diener, J.F.A. (2014) On parameterizing thermodynamic descriptions of minerals for petrological calculations. Journal of Metamorphic Geology, 32(3), 245-260.

Salmon, M., Kennett, B.L.N., Stern, T., and Aitken, A.R.A. (2013) The Moho in Australia and New Zealand. Tectonophysics, 609, 288-298.

Schumacher, J.C. (1991a) Empirical Ferric Iron Corrections - Necessity, Assumptions, and Effects on Selected Geothermobarometers. Mineralogical Magazine, 55(378), 3-18.

Schumacher, J.C. (1991b) Empirical ferric iron corrections: necessity, assumptions, and effects on selected geothermobarometers. Mineralogical Magazine, 55(378), 3-18.

Selway, K. (2019) Electrical Discontinuities in the Continental Lithosphere Imaged with Magnetotellurics. Lithospheric Discontinuities, 239, 89-109.

Selway, K., Ford, H., and Kelemen, P. (2015) The seismic mid-lithosphere discontinuity. Earth and Planetary Science Letters, 414, 45-57.

Skogby, H. (2006) Water in natural mantle minerals I: pyroxenes. In H. Keppler, and J.R. Smyth, Eds. Water in Nominally Anhydrous Minerals, 62, p. 155-167. Mineralogical Society of America.

Stagno, V., Ojwang, D.O., McCammon, C.A., and Frost, D.J. (2013) The oxidation state of the mantle and the extraction of carbon from Earth's interior. Nature, 493(7430), 84-+.

Stalder, R., Klemme, S., Ludwig, T., and Skogby, H. (2005) Hydrogen incorporation in orthopyroxene: interaction of different trivalent cations. Contributions to Mineralogy and Petrology, 150(5), 473-485.

Stalder, R., Kronz, A., and Simon, K. (2008) Hydrogen incorporation in enstatite in the system MgO-SiO2-H2O-NaCl. Contributions to Mineralogy and Petrology, 156(5), 653-659.

929 Tarits, P., Hautot, S., and Perrier, F. (2004) Water in the mantle: Results from electrical
930 conductivity beneath the French Alps. Geophysical Research Letters, 31(6).

931 Taylor, W. (1998) An experimental test of some geothermometer and geobarometer formulations
932 for upper mantle peridotites with application to the thermobarometry of fertile lherzorite
933 and garnet websterite. Neues Jahrbuch feur Mineralogie Abhandlungen, 172, 381-408.

934 Tielke, J.A., Zimmerman, M.E., and Kohlstedt, D.L. (2017) Hydrolytic weakening in olivine
935 single crystals. Journal of Geophysical Research-Solid Earth, 122(5), 3465-3479.

936 Tollan, P.M.E., Smith, R., O'Neill, H.S.C., and Hermann, J. (2017) The responses of the four
937 main substitution mechanisms of H in olivine to H2O activity at 1050 degrees C and 3
938 GPa. Progress in Earth and Planetary Science, 4.

939 Valley, J.W., Bohlen, S.R., Essene, E.J., and Lamb, W. (1990) Metamorphism in the
940 Adirondacks .2. The Role of Fluids. Journal of Petrology, 31(3), 555-596.

941 Wagner, C., Deloule, E., and Mokhtari, A. (1996) Richterite-bearing peridotites and MARID-
942 type inclusions in lavas from North Eastern Morocco: Mineralogy and D/H isotopic
943 studies. Contributions to Mineralogy and Petrology, 124(3-4), 406-421.

944 Wallis, D., Hansen, L.N., Tasaka, M., Kumamoto, K.M., Parsons, A.J., Lloyd, G.E., Kohlstedt,
945 D.L., and Wilkinson, A.J. (2019) The impact of water on slip system activity in olivine
946 and the formation of bimodal crystallographic preferred orientations. Earth and Planetary
947 Science Letters, 508, 51-61.

948 Wang, D.J., Li, H.P., Yi, L., and Shi, B.P. (2008) The electrical conductivity of upper-mantle
949 rocks: water content in the upper mantle. Physics and Chemistry of Minerals, 35(3), 157-
950 162.

951 Wells, P.R.A. (1977) Pyroxene Thermometry in Simple and Complex Systems. Contributions to
952 Mineralogy and Petrology, 62(2), 129-139.

953 White, R.W., Powell, R., Holland, T.J.B., Johnson, T.E., and Green, E.C.R. (2014) New mineral
954 activity-composition relations for thermodynamic calculations in metapelitic systems.
955 Journal of Metamorphic Geology, 32(3), 261-286.

956 Wood, B.J. (1974) Solubility of Alumina in Orthopyroxene Coexisting with Garnet.
957 Contributions to Mineralogy and Petrology, 46(1), 1-15.

958 -. (1990a) An Experimental Test of the Spinel Peridotite Oxygen Barometer. Journal of
959 Geophysical Research-Solid Earth and Planets, 95(B10), 15845-15851.

960 Wood, B.J. (1990b) An experimental test of the spinel peridotite oxygen barometer. Journal of
961 Geophysical Research, 95(B10), 15845-15851.

962 Wood, B.J., Bryndzia, L.T., and Johnson, K.E. (1990) Mantle oxidation state and its relationship
963 to tectonic environment and fluid speciation. Science, 248(4953), 337-345.

964 Wood, B.J., and Virgo, D. (1989) Upper mantle oxidation state: Ferric iron contents of lherzolite
965 spinels by ^{57}Fe Mossbauer spectroscopy and resultant oxygen fugacities. Geochimica et
966 Cosmochimica Acta, 53, 1277-1291.

967 Woodland, A.B., and Koch, M. (2003) Variation in oxygen fugacity with depth in the upper
968 mantle beneath the Kaapvaal craton, Southern Africa. Earth and Planetary Science
969 Letters, 214(1–2), 295-310.

970 Woodland, A.B., Kornprobst, J., and Tabit, A. (2006) Ferric iron in orogenic lherzolite massifs
971 and controls of oxygen fugacity in the upper mantle. Lithos, 89(1-2), 222-241.

972 Woodland, A.B., Kornprobst, J., and Wood, B.J. (1992) Oxygen thermobarometry of orogenic
973 lherzolite massifs. Journal of Petrology, 33(1), 203-230.

974 Zhang, C., and Duan, Z.H. (2009) A model for C-O-H fluid in the Earth's mantle. Geochimica Et
975 Cosmochimica Acta, 73(7), 2089-2102.

976 Zhao, Y.-H., Ginsberg, S.B., and Kohlstedt, D.L. (2004) Solubility of hydrogen in olivine:
977 dependence on temperature and iron content. Contributions of Mineralogy and Petrology,
978 147, 155-161.
979
980

Figure Captions:

Figure 1: Map of Southeastern Australia illustrating the xenolith location. These samples were collected from volcanics erupted from the Bullenmerri and Gnotuk Maars.

Figure 2: Images illustrating the mineralogy and textures of samples examined in this study. Abbreviations: A – amphibole; C – clinopyroxene; O – orthopyroxene; Ol – olivine; S – spinel. 2A. Sample GN9912 with multigrain aggregates of amphibole that often surround spinel. The rectangle labeled B is equivalent to the photomicrograph in the lower righthand corner of this image. 2B) A photomicrograph of sample GN9912 from the box labeled "B" on image 2A. This illustrates that amphibole may rim clinopyroxene (cpx) in addition to spinel. 2C: Sample BM9915 also has amphibole surrounding spinel, but the amount of amphibole is small relative to spinel as compared to samples GN9912 and GN9913. 2D). In this sample amphibole is largely present as individual grains that are not clearly associated with spine or cpx.

Figure 3: Mineral compositions plotted as a function of distance within individual mineral grains; vertical axes represent locations of grain boundaries. (a) Relative depletion in Al and enrichment in Si and Mg is sometimes apparent at grain boundaries as illustrated by this opx grain from GN9913. (b) Compositions of a spinel grain from sample BM9912 with rims enriched in Cr and depleted in Al.

Figure 4. T–aH$_2$O stability of equilibrium1 (pargasite), and 2 (tremolite) illustrating estimation of values of aH$_2$O using sample BM9915 as an example (P = 1.3 GPa). Solid lines and closed symbols illustrate the stability of these equilibria for minimum oxy-amphibole contents ($Fe^{3+}/\Sigma Fe = 0$) while dashed lines and open symbols indicate stability based on maximum oxy-amphibole contents ($Fe^{3+}/\Sigma Fe = 1$). Thus, the value of aH$_2$O recorded by sample BM9915 (910 ˚C) falls between 0.06 and 0.13. Consideration of the uncertainty involved in aH$_2$O estimates based on equilibrium (2) indicate values of aH$_2$O may fall between 0.03 to 0.27 (hexagonal symbols). Even though uncertainties related to the stability of equilibrium (1) is ≈ ± 350 ˚C, the estimate of aH$_2$O with this equilibrium indicates a value of aH$_2$O < 0.15.

Figure 5. Values of aH_2O estimated using equilibrium (1) and equilibrium (2), determined using both minimum oxy-amphibole contents ($Fe^{3+}/\Sigma Fe = 0$, closed symbols) and maximum oxy-amphibole contents ($Fe^{3+}/\Sigma Fe = 1$, open symbols).

Figure 6. Mole fractions of CO_2, H_2O (dashed), and CH_4 plotted as a function of oxygen fugacity at 820 ˚C and 11 kbar (1.1GPa) in both the graphite bearing system (aC = 1, top), and a system in which aC is reduced (aC = 0.1 bottom). The vertical black line represents the maximum stability of graphite (top - aC < 1 at fO_2 more oxidizing than this line), and the analogous line on the bottom figure is placed at fO_2 above which aC must be less than 0.1. The vertical dashed line represents the value of oxygen fugacity recorded by sample GN9912, indicating that a lithostatically pressured C-O-H fluid at this oxygen fugacity should be H_2O rich. H_2 and CO are not plotted as the mole fraction of either of these species is always < 0.02 for the P-T and values of fO_2 shown here.

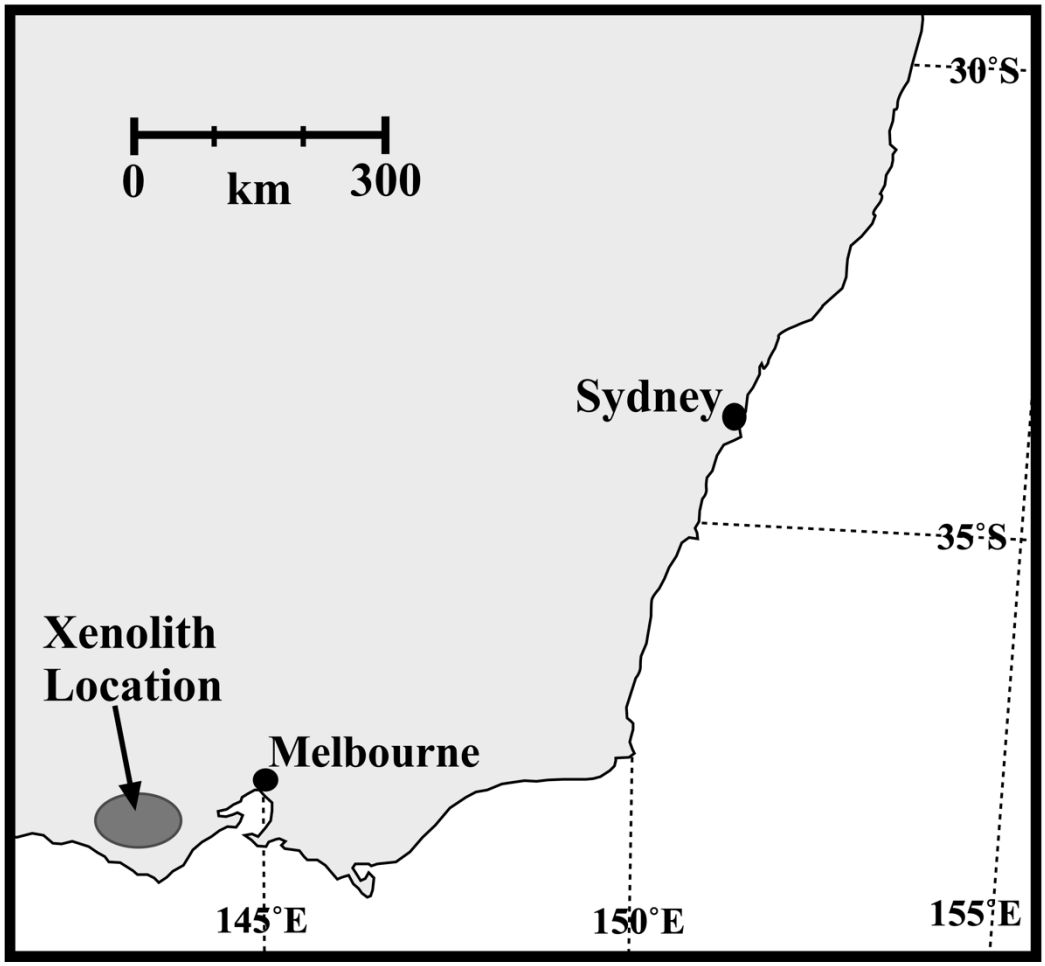

Figure 1.

This is the peer-reviewed, final accepted version for American Mineralogist, published by the Mineralogical Society of America.
The published version is subject to change. Cite as Authors (Year) Title. American Mineralogist, in press.
DOI: https://doi.org/10.2138/am-2022-8735. http://www.minsocam.org/

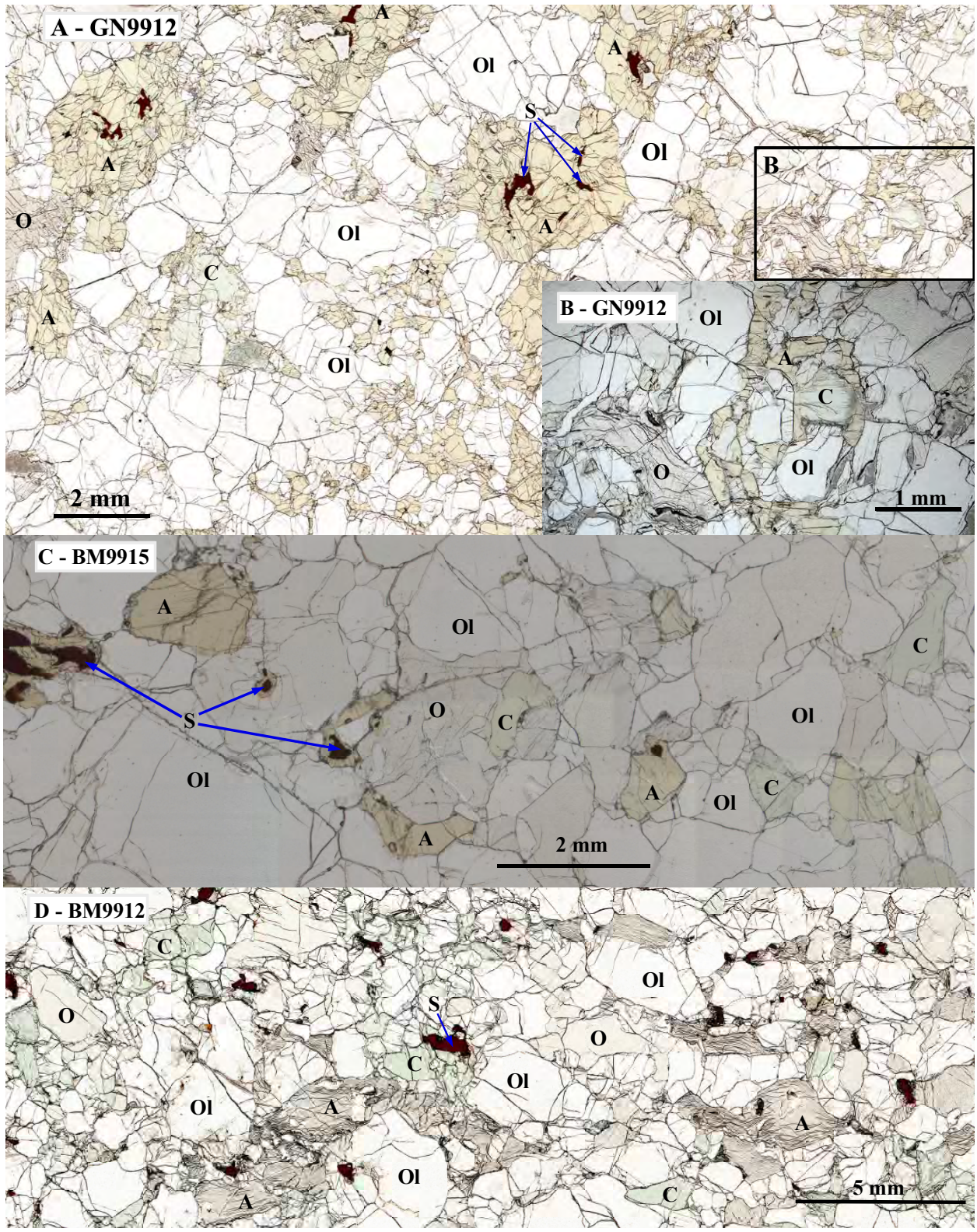

Figure 2.

This is the peer-reviewed, final accepted version for American Mineralogist, published by the Mineralogical Society of America.
The published version is subject to change. Cite as Authors (Year) Title. American Mineralogist, in press.
DOI: https://doi.org/10.2138/am-2022-8735. http://www.minsocam.org/

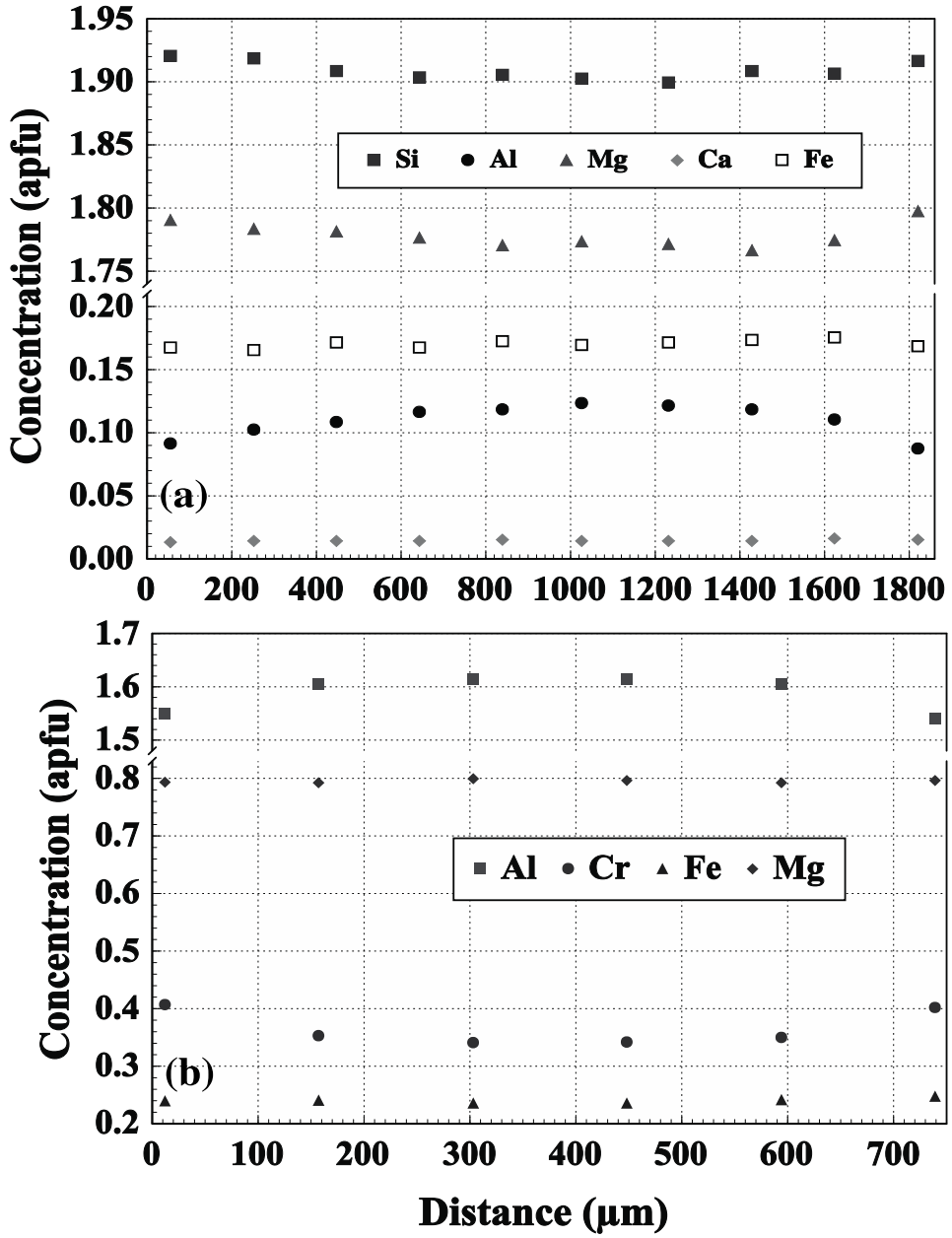

Figure 3:

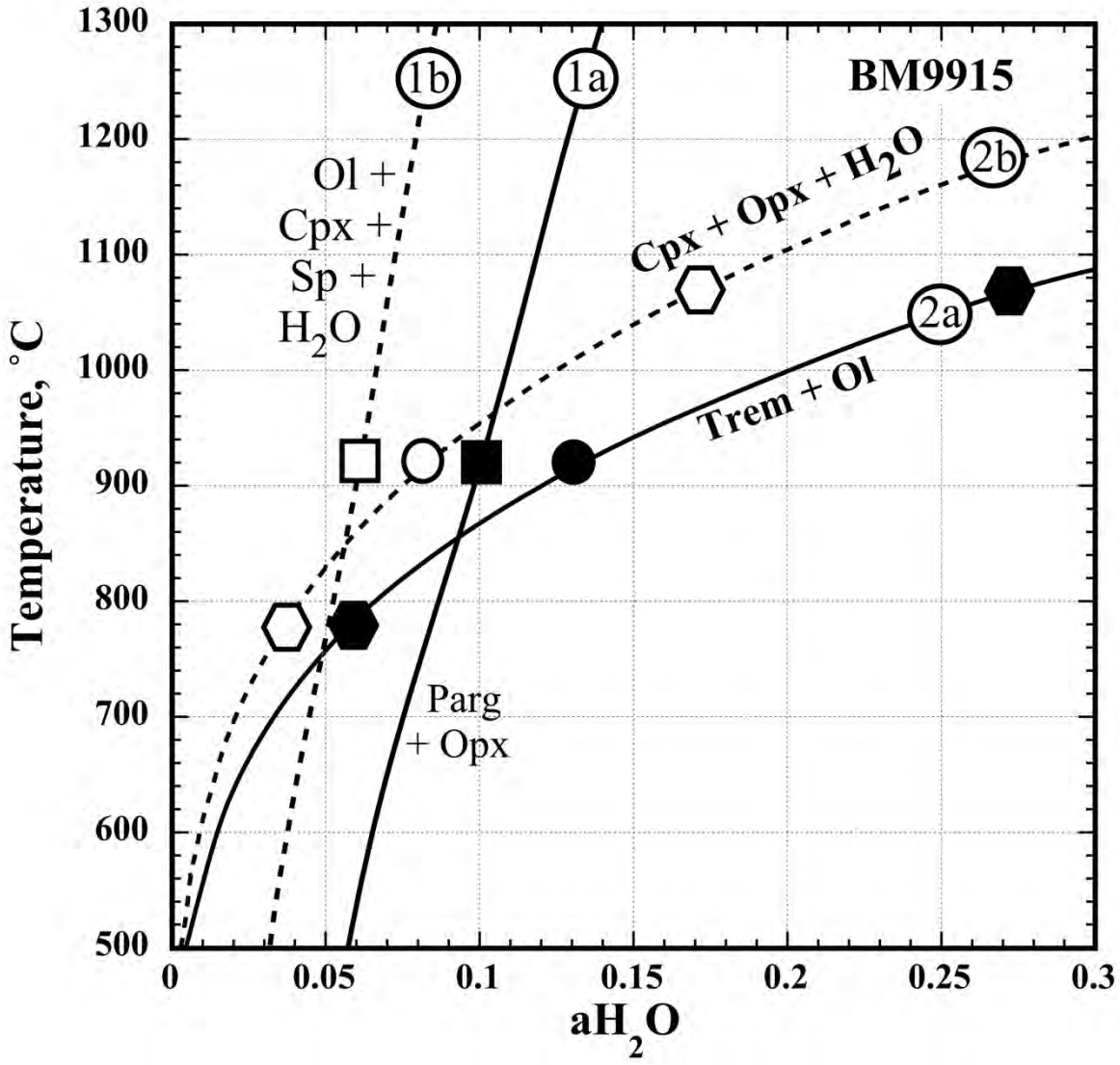

Figure 4.

This is the peer-reviewed, final accepted version for American Mineralogist, published by the Mineralogical Society of America.
The published version is subject to change. Cite as Authors (Year) Title. American Mineralogist, in press.
DOI: https://doi.org/10.2138/am-2022-8735. http://www.minsocam.org/

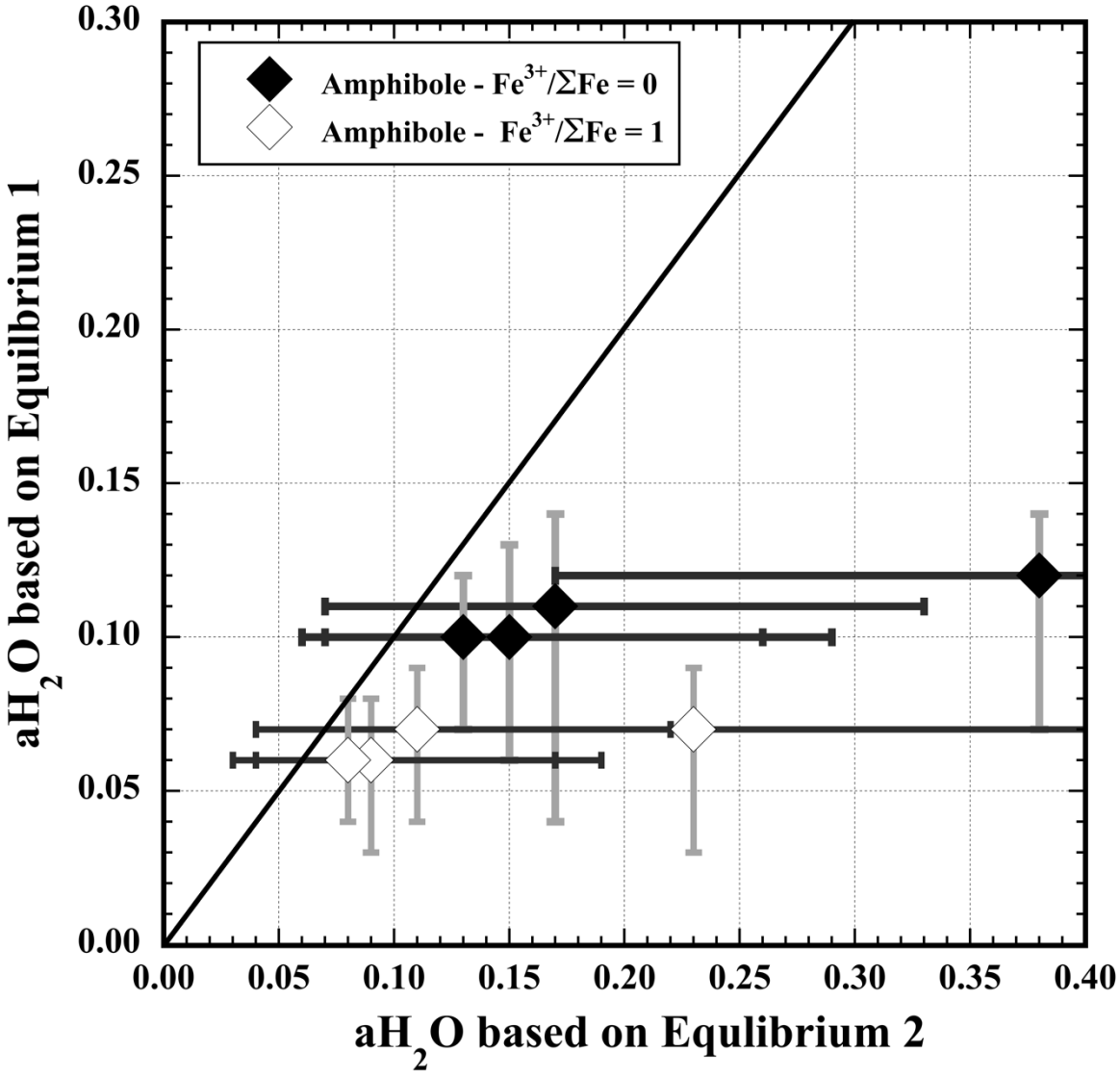

Figure 5.

1079

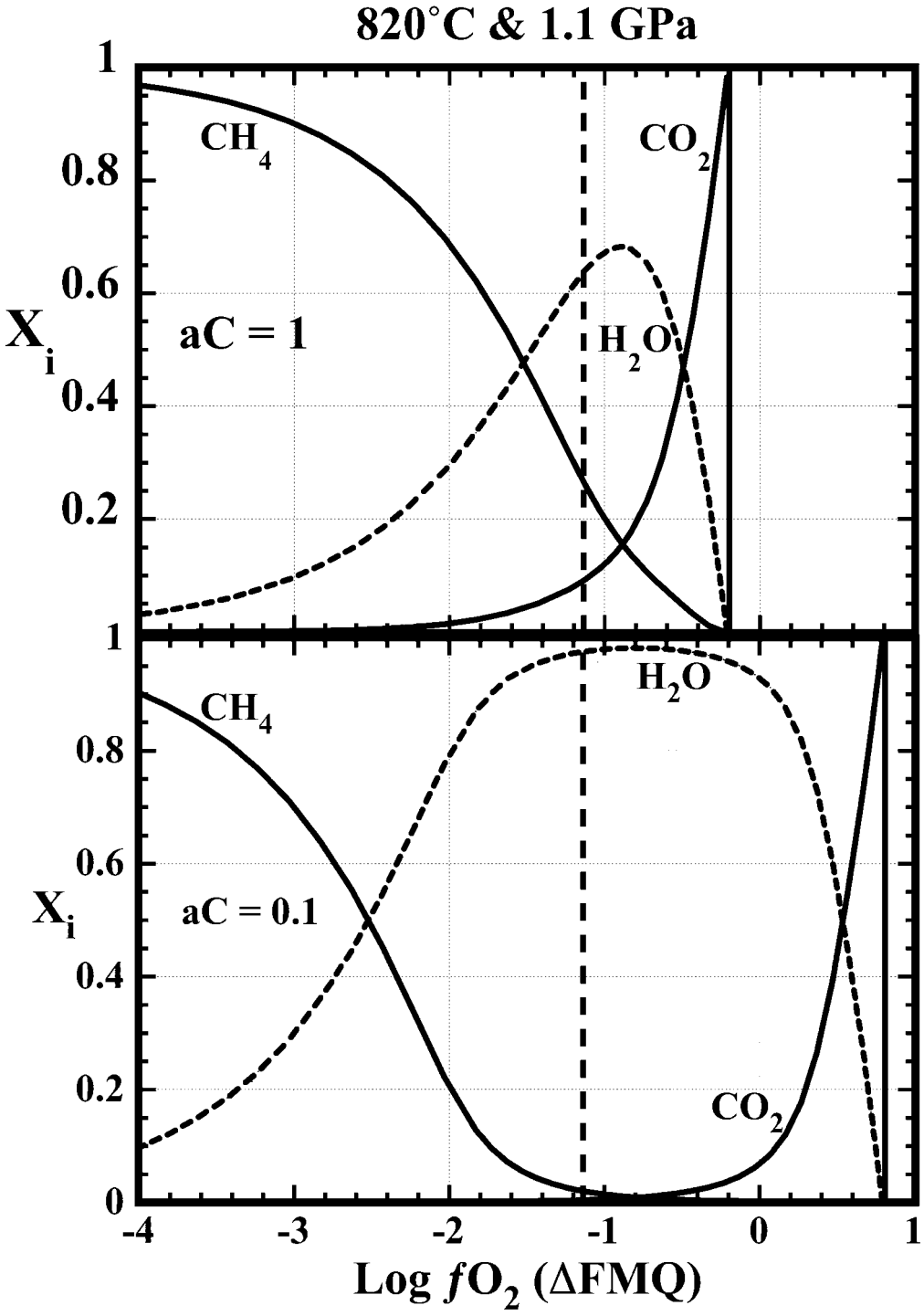

1080
1081
1082
1083 Figure 6
1084

This is the peer-reviewed, final accepted version for American Mineralogist, published by the Mineralogical Society of America.
The published version is subject to change. Cite as Authors (Year) Title. American Mineralogist, in press.
DOI: https://doi.org/10.2138/am-2022-8735. http://www.minsocam.org/

Table 1. Temperature (˚C) and Pressure (GPa) estimates

Sample:	T(98)[a]	BK[b]	NT[c]	BKNG[d]	Wells[e]	P
BM9912	**920**	920	930	900	960	1.4
BM9915	**910**	890	920	860	960	1.3
GN9912	**820**	800	830	740	880	1.1
GN9913	**850**	840	860	790	910	1.1

Two-pyroxene temperatures: (a) Taylor (1998), (b) Brey & Kohler (1990), Ca-in-opx, (c) Nimis and Taylor (2000) En-in-cpx, (d) Nimis and Grutter (2010) modified B&K Ca-in-opx, (e) Wells (1977)

Table 2. Activities of mineral end members and H_2O.

Equilibrium 2 - Tremolite						Uncertainty		Uncertainty
	aFo	aDi	aEn	aTr	aH_2O[1]	aH_2O ±	aH_2O[2]	aH_2O ±
BM9912	0.82	0.65	0.76	0.04	0.38	-0.21, +0.31	0.23	-0.12, +0.22
BM9915	0.84	0.71	0.77	0.02	0.13	-0.07, +0.13	0.08	-0.05, +0.09
GN9912	0.79	0.71	0.77	0.04	0.15	-0.08, +0.14	0.09	-0.05, +0.10
GN9913	0.82	0.72	0.81	0.05	0.17	-0.1, +0.16	0.11	-0.07, +0.11
Equilibrium 1 - Pargasite								
	Fo/Di/En	aJd	aSp	aParg	aH_2O[1]	aH_2O ±	aH_2O[2]	aH_2O ±
BM9912	SA*	0.11	0.63	0.26	0.12	-0.05, +0.02	0.07	-0.04, +0.02
BM9915	SA*	0.08	0.58	0.19	0.10	-0.03, +0.02	0.06	-0.02, +0.02
GN9912	SA*	0.10	0.59	0.28	0.10	-0.04, +0.03	0.06	-0.03, +0.02
GN9913	SA*	0.09	0.61	0.29	0.11	-0.07, +0.03	0.07	-0.03, +0.02

* SA - Activities of Fo, Di, and En are the same as above (SA); i.e., see equilibria 2.

1 - aH_2O based on amphibole normalization with $Fe^{3+}/\Sigma Fe=0$

2 - aH_2O based on amphibole normalization with $Fe^{3+}/\Sigma Fe=1$

Table 3: Values of fO_2 with maximum XH_2O and minimum values of XCO_2 and XCH_4

	Miller et al. (2016)		Bryndzia & Wood (1990)		Max.	Min.	Max.
Sample	$\Delta Log fO_2$*	Log fO_2	$\Delta Log fO_2$*	Log fO_2	XCO_2	XH_2O	XCH_4
BM9912	-0.33	-11.64	-0.27	-11.57	NA	NA	NA
BM9915	-0.20	-11.75	-0.18	-11.72	NA	NA	NA
GN9912	-1.16	-14.53	-1.24	-14.61	0.08	0.63	0.28
GN9913	-0.21	-13.01	-0.36	-13.15	NA	NA	NA

* Relative to FMQ